International Journal of Solids and Structures 193–194 (2020) 418–433

Contents lists available at ScienceDirect

International Journal of Solids and Structures

journal homepage: www.elsevier.com/locate/ijsolstr

A model for hyperelastic materials reinforced with fibers resistance to extension and flexure

Suprabha Islam[a], Dinara Zhalmuratova[b], Hyun-Joong Chung[b], Chun IL Kim[b,*]

[a] Department of Mechanical Engineering, University of Alberta, Edmonton, Alberta T6G 1H9, Canada
[b] Department of Chemical and Materials Engineering, University of Alberta, Edmonton, Alberta T6G 1H9, Canada

ARTICLE INFO

Article history:
Received 27 September 2019
Revised 17 February 2020
Accepted 25 February 2020
Available online 26 February 2020

Keywords:
Finite plane deformations
Soft hyperelastic material
J-shaped stress-strain response
Elastomeric composites
Strain gradient theory

ABSTRACT

A model for the mechanics of a soft hyperelastic material reinforced with long fibers is presented in finite plane elastostatics. The strain energy potential of the composite is refined by the Mooney Rivlin model to accommodate the hyperelastic behaviors of the matrix material. Within the framework of the strain gradient theory, the kinematics of the fibers is formulated and subsequently integrated into the model of continuum deformation. A rigorous derivation of the Euler equation and the associated boundary conditions are presented by virtue of variational principles and a virtual work statement. In particular, the obtained model successfully predicts the 'J-shaped' stress-strain responses, deformation profiles and shear strain angles of the elastomer - polyester fiber composites subjected to uniaxial extension. The proposed model may also serve as an alternative of the Holzapfel model in the design and analysis of biomimetic composites with rapid strain-stiffening behaviors by providing direct estimations of the stress-strain responses of intended composites.

1. Introduction

Elastomeric materials reinforced with fibers (elastomeric composites) have consistently been the subject of intense study (Shao et al., 2018; Bouillaguet et al., 2006; Bailly et al., 2014; Leong et al., 2000; Maurer et al., 2015) for their practical importance in biomaterial science and engineering. Contemporary applications of elastomeric composites include the areas of tissue engineering, microfluidics and biomechanics (Wang et al., 2018; Cheng et al., 2010; Pritts and Rahn, 2004). For example, in soft robotics, progress is being made to replace conventional materials (e.g. rigid polymer, ceramics, metals etc...) with the elastomeric composites in order to achieve more sophisticated functionalities such as manipulation of delicate objects, conformation to surroundings, and adoptive movement in various environments (Martinez et al., 2013). When the elastomeric matrix materials are used in conjunction with systematically arranged fiber families they form highly elastic materials that display direction-dependent properties (orthotropic properties) and sustain rapid strain stiffening response at low strain level (20%–50%), known as '*J-shaped*' stress-strain behavior (Shadwick, 1999). In fact, *J-shaped* and orthotropic stress-strain behaviors are the characteristics of the biological materials such as blood vessels, tendons, muscles, skin and ligaments (Fung, 1984; Vatankhah-Varnosfaderani et al., 2017). This, in turn, suggests that biological tissues may be mimicked via the systematic adjustment and/or optimization of the mechanical responses of elastomeric composites. Such practices include the predictions and characterizations of the resultant responses of elastomeric composites from the individual properties of elastomeric matrixes and fibers, which are also in a period of active study (Yan et al., 2017; Myung et al., 2007; Ma et al., 2017). Authors in Holzapfel et al. (2000) proposed a model to describe the fabric-reinforced behavior of a multi-walled structure of elastic artery. Gent's and Mooney Rivlin model are also widely adopted to directly fit the *J-shaped* stress-strain curves measured from the resulting elastomeric composites (Gent, 1996; Lu et al., 2012; Zhao and Wang, 2014). These models may be employed in the combined sense (e.g. Gent's constitutive model used in conjunction with Holzapfel model) to achieve more accurate predictions and/or fittings Zhalmuratova et al..

On the other hand, a continuum-based model which incorporates the responses of fibers into the model of the continuum deformation may be sought as a promising alternative. This is framed in the setting of the nonlinear strain gradient theory (Toupin, 1964; Koiter, 1964; Truesdell and Noll, 1965) of anisotropic elasticity in which the fibers' bending resistance is assigned to the changes in curvature (flexure) of fibers explicitly (Spencer and Soldatos, 2007). The latter is obtained via the computation of the second gradient of deformations prescribed on the convected

* Corresponding author.
E-mail addresses: cikim@ualberta.ca, cikim1007@naover.com (C.I. Kim).

https://doi.org/10.1016/j.ijsolstr.2020.02.036
0020-7683/

curves of continuously distributed fibers. The concept is further refined to accommodate fibers resistant to flexure, extension and twist within the context of the Cosserat theory of non-linear elasticity (Steigmann, 2012). The second gradient-based continuum models have been successfully adopted in a wide range of engineering problems such as the mechanics of meshed structures (Dell'Isola et al., 2016b; 2017; 2016a), bending of unidirectional and bidirectional fiber composites (Zeidi and Kim, 2017a; 2018; Kim, 2019) and composites reinforced with extensible fibers (Zeidi and Kim, 2017b). To this end, authors in Kim and Zeidi (2018) presented the continuum formulation for the description of the bidirectional fiber-reinforced composites, which results in the smooth transitions of shear strain distributions. However, the models developed in Zeidi and Kim (2017a, 2018); Kim (2019); Zeidi and Kim (2017b); Kim and Zeidi (2018) may not be ideal for the analysis of highly strained fiber-elastomer composites, since the analyses in Zeidi and Kim (2017a, 2018); Kim (2019); Zeidi and Kim (2017b); Kim and Zeidi (2018) are intrinsically limited to relatively ' *small*' deformation regime where linear stress-strain responses are dominant.

In the present study, we develop a continuum-based model which describes hyperelastic responses of elastomeric matrix materials reinforced with polyester fibers and subjected to finite plane deformations. Thus, it is assumed that the fiber's directors remain in a plane, with no out-of-plane components and that the corresponding deformations and material parameters are independent of the out-of-plane coordinate. Emphasis is placed on the assimilation of rapid strain-stiffening responses of the elastomeric composites at the lower strain levels while maintaining the rigor and generality in the derivation of the associated constitutive formulation. The strain energy potential of the composite is refined by the Mooney Rivlin strain energy function, which is one of the widely adopted strain energy model for the descriptions of materials sustaining large deformations analyses (see, for example, Ogden, 1984; Steigmann, 2017). Within the framework of the second gradient theory, the kinematics of fibers are determined by their position and direction fields and incorporated into the model of continuum deformation while considering fibers as continuously distributed spatial rods of Kirchhoff type (Landau and Lifshitz, 1986; Dill, 1992; Antman, 2005). The Euler equilibrium equations and the associated boundary conditions are also derived by means of a virtual work statement and variational principles of the second gradient of deformations. The solutions of the resulting Partial Differential Equations (PDEs) are obtained via the custom-built numerical procedures, which demonstrate close correspondence with the results in literature Zhalmuratova et al., (Dell'Isola et al., 2017) and (Dell'Isola et al., 2016a).

More importantly, the obtained model assimilates the responses of the *Ecoflex 00500* elastomer – fiber composite subjected to uniaxial tension and successfully predicts the *J-shaped* stress-strain behavior. To further examine the performance of the obtained model, we also compare it to the Neo Hookean – Holzapfel model (Holzapfel et al., 2000), Zhalmuratova et al. and (Holzapfel, 2008). It turns out that both the proposed model and Holzapfel model perform well in the estimations of *J-shaped* stress-strain responses of the samples in which the strain-stiffening phenomena is less significant. For the composites with rapid strain-stiffening responses, the proposed model produces more accurate prediction results than the Holzapfel model at low strain levels. In particular, the proposed model directly predicts the resultant stress-strain responses of the composite by integrating the predetermined modulus of matrix materials and fibers into the model of continuum deformation. This may facilitate the design and analysis of a particular composite by providing the instant estimations of the mechanical responses of intended composites. In addition to the stress-strain responses of the composites, the obtained model provides the estimations of other important design considerations such as deformation profiles and contours, and the smooth transitions in the shear strain fields. Potential applications may also include failure analysis of highly strained fiber-elastomer composites, since the model estimates the shear strain fields of the desired composites from which the corresponding shear energy distributions can be obtained.

Throughout the manuscript, we use standard notation such as $\mathbf{A}^T$, $\mathbf{A}^{-1}$, $\mathbf{A}^*$ and $tr(\mathbf{A})$. These are the transpose, the inverse, the cofactor and the trace of a tensor $\mathbf{A}$, respectively. The tensor product of vectors is indicated by interposing the symbol $\otimes$, and the Euclidian inner product of tensors $\mathbf{A}$, $\mathbf{B}$ is defined by $\mathbf{A}\cdot\mathbf{B} = tr(\mathbf{A}\mathbf{B}^T)$; the associated norm is $|\mathbf{A}| = \sqrt{\mathbf{A}\cdot\mathbf{A}}$. The symbol $|\cdot|$ is also used to denote the usual Euclidian norm of vectors. Latin and Greek indices take values in {1, 2} and, when repeated, are summed over their ranges. Lastly, the notation $F_{\mathbf{A}}$ stands for the tensor-valued derivatives of a scalar-valued function $F(\mathbf{A})$.

2. Kinematics

Our intention throughout this section is to establish the kinematic framework that will be used in the constitutive formulations of hyperelastic matrix-fiber composites. We note that, in the forgoing development, unidirectional fiber-reinforced composites are considered for the sake of simplicity. The cases of bidirectional fibers can be readily accommodated via similar approaches, as done in Kim and Zeidi (2018) and Steigmann and dell'Isola (2015).

Let $\mathbf{r}(s)$ be the parametric curve which represents the fibers' trajectory on the deformed configuration and $\boldsymbol{\tau}$ be the unit tangent in the direction of increasing s. We also assign $\mathbf{X}(S)$ and S as their counter parts in the reference configuration. The orientation of a particular fiber is then defined by

$$\Lambda = |\mathbf{d}| \text{ and } \Lambda\boldsymbol{\tau} = \mathbf{d};\ \Lambda \equiv \frac{ds}{dS} \text{ and } \tau \equiv \frac{d\mathbf{r}(s)}{ds}, \tag{1}$$

where

$$\mathbf{d} = \mathbf{F}\mathbf{D},\ \mathbf{F} = \boldsymbol{\Lambda}\boldsymbol{\tau}\otimes\mathbf{D}, \tag{2}$$

and $\mathbf{F}$ is the gradient of the deformation function ($\boldsymbol{\chi}(\mathbf{X})$). Eq. (2) is obtained by taking the derivative of $\mathbf{r}(s(S)) = \chi(\mathbf{X}(S))$ with respect to arc length parameters S and s, upon making the identifications $\mathbf{D} = d\mathbf{X}/dS$. Here, $d(\mathbf{*})/dS$ and $d(\mathbf{*})/ds$ refer to the arc length derivatives of $(^*)$ along the fibers' directions in the reference and deformed configurations, respectively. Eq. (2) can be projected using the orthonormal bases of $\{\mathbf{E}_A$: *reference*$\}$ and $\{\mathbf{e}_i$: *current*$\}$ to yield

$$\Lambda\tau_i = d_i = F_{iA}D_A \text{ for } \mathbf{D} = D_A\mathbf{E}_A \text{ and } \mathbf{d} = d\mathbf{e}_i, \tag{3}$$

which may also be used in the later sections.

Thus, from Eqs. (1)–(2), the expression for geodesic curvature of a parametric curve ($\mathbf{r}(s)$) is obtained by

$$\mathbf{g} \equiv \mathbf{r}'' = \frac{d\left(\frac{d\mathbf{r}(S)}{dS}\right)}{dS} = \frac{\partial(\mathbf{F}\mathbf{D})}{\partial\mathbf{X}}\frac{\partial\mathbf{X}}{\partial S} = \nabla[\mathbf{F}\mathbf{D}]\mathbf{D}. \tag{4}$$

In a typical environment, most of the fibers are straight prior to deformations. Even slightly curved fibers can be idealized as 'fairly straight' fibers, considering their length scales with respect to those of the matrix materials. This indicates that the gradients of unit tangents in the reference configuration identically vanish (i.e. $\nabla\mathbf{D} = 0$). Accordingly, Eqs. (4) reduces to

$$\mathbf{g} = \nabla\mathbf{F}(\mathbf{D}\otimes\mathbf{D}) = \mathbf{G}(\mathbf{D}\otimes\mathbf{D}), \tag{5}$$

where we adopt the convention of the second gradient of deformations as

$$\nabla\mathbf{F} \equiv \mathbf{G}, \tag{6}$$

and the compatibility condition of $\mathbf{G}$ is given by

$$G_{iAB} = F_{iA,B} = F_{iB,A} = G_{iBA}. \tag{7}$$

The forgoing developments imply that the response of fiber-reinforced materials are governed by both the first and second gradient of deformations such that

$$W(\mathbf{F},\mathbf{G}) = \widehat{W}(\mathbf{F}) + W(\mathbf{G}), \quad W(\mathbf{G}) \equiv \frac{1}{2}C(\mathbf{F})|\mathbf{g}|^2, \tag{8}$$

where $C(\mathbf{F})$ refers to the material property associated with the bending motions of fibers, which are generally independent of the deformation gradient (i.e. $C(\mathbf{F}) = C$). Further, $\mathbf{g}$ is the geodesic curvature of fibers which is computed via the second gradient of continuum deformation (G). Eq. (8) is consistent with the model proposed by Spencer and Soldatos (2007) that, in the case of a single family of fibers, the dependence of the strain energy on $\mathbf{G}$ occurs through $\mathbf{g}$; i.e.,

$$W(\mathbf{G}) = W(\mathbf{g}(\mathbf{G})). \tag{9}$$

The invariance requirements arising in the second gradient continuum deformation remain valid for cases of finite elastic deformations of continuum bodies (Spencer, 1972; 1984; Rivlin, 1995) and biological membranes subjected to large deformations (Holzapfel and Ogden, 2006), and therefore, have been adopted in the present study without further proof. For the desired applications, we now introduce the strain energy potential, which addresses the fiber's resistance to extension as

$$W(\varepsilon) = \frac{1}{2}E\varepsilon^2, \tag{10}$$

where the expression of ε is given by

$$\varepsilon = \frac{1}{2}(\Lambda^2 - 1), \tag{11}$$

and E is a modulus pertaining to the fiber's extension. Further, in view of Eq. ((3), Λ^2 can be expressed in terms of the deformation gradient tensor $\mathbf{F}$ and the director field of fibers $\mathbf{D}$ as

$$\Lambda^2 = \mathbf{FD}\cdot\mathbf{FD} = \mathbf{F}^T\mathbf{FD}\cdot\mathbf{D} = (\mathbf{F^TF})\cdot\mathbf{D}\otimes\mathbf{D}. \tag{12}$$

It is clear from Eqs. (11) and (12) that the fiber's extension is $\mathbf{F}$-dependent via ε (i.e. $\varepsilon = \varepsilon(\mathbf{F})$) and thus the strain energy function (Eq. (8)) can be augmented by Eq. (10) to yield

$$W(\mathbf{F},\varepsilon(\mathbf{F}),\mathbf{g}(\mathbf{G})) = \widehat{W}(\mathbf{F}) + \frac{1}{2}E\varepsilon^2 + \frac{1}{2}C|\mathbf{g}(\mathbf{G})|^2. \tag{13}$$

We also note that the torsional energy of the fibers is excluded in the present study, since the in-plane deformation (plane strain) of the fiber composites is considered. Further, it is discussed in Spencer and Soldatos (2007) that the indeterminacy arising in the plane strain formulations of the second gradient of deformations results no effects on the associated energy balance equation and is not case specific to fiber-reinforced materials. The related derivations and discussions can be found in Toupin (1962); Mindlin and Tiersten (1962a). In the present study, we simply adopt the results for the sake of conciseness. For uses in the derivation of Euler equations and the associated boundary conditions, we continue by evaluating the induced energy variation of the response function (Eq. (13)) with respect to $\mathbf{F}$, ε, and $\mathbf{g}$ as

$$\dot{W}(\mathbf{F},\varepsilon,\mathbf{g}) = W_{\mathbf{F}}\cdot\dot{\mathbf{F}} + W_\varepsilon\dot{\varepsilon} + W_{\mathbf{g}}\cdot\dot{\mathbf{g}}. \tag{14}$$

In the above, the superposed dot refers to derivatives with respect to a parameter ε at the particular configuration of the composite (i.e. $\varepsilon = 0$) that labels a one-parameter family of deformations.

The desired expressions for the energy variation can be obtained from Eqs. (10)–(13) that

$$\dot{\varepsilon} = \frac{1}{2}(\Lambda^2 - 1)\dot{} = \frac{1}{2}(\mathbf{FD}\cdot\mathbf{FD} - \mathbf{1})\dot{} = \mathbf{FD}\cdot\dot{\mathbf{F}}\mathbf{D} = \mathbf{FD}\otimes\mathbf{D}\cdot\dot{\mathbf{F}}, \tag{15}$$

$$W_\varepsilon = E\varepsilon, \text{ and } W_{\mathbf{g}} = C\mathbf{g}. \tag{16}$$

The above further leads to

$$W_\varepsilon\dot{\varepsilon} = E\varepsilon\dot{\varepsilon} = E[\frac{1}{2}\{(\mathbf{F^TF})\cdot\mathbf{D}\otimes\mathbf{D} - 1\}][\mathbf{FD}\otimes\mathbf{D}]\cdot\dot{\mathbf{F}} \tag{17}$$

$$W_{\mathbf{g}}\dot{\mathbf{g}} = C\mathbf{g}\cdot\dot{\mathbf{g}} = \mathbf{G}(\mathbf{D}\otimes\mathbf{D})\cdot\dot{\mathbf{G}}(\mathbf{D}\otimes\mathbf{D}) = (C\mathbf{g}\otimes\mathbf{D}\otimes\mathbf{D})\cdot\dot{\mathbf{G}}, \tag{18}$$

where $\mathbf{g} = \mathbf{G}(\mathbf{D}\otimes\mathbf{D})$ (see, Eq. (5)).

Finally, combining Eqs. (14)–(18), we find

$$\dot{W}(\mathbf{F},\varepsilon,\mathbf{g}) = W_{\mathbf{F}}\cdot\dot{\mathbf{F}} + E[\frac{1}{2}\{(\mathbf{F^TF})\cdot\mathbf{D}\otimes\mathbf{D} - 1\}][\mathbf{FD}\otimes\mathbf{D}]\cdot\dot{\mathbf{F}} + (C\mathbf{g}\otimes\mathbf{D}\otimes\mathbf{D})\cdot\dot{\mathbf{G}}. \tag{19}$$

or equivalently

$$\dot{W}(\mathbf{F},\varepsilon,\mathbf{g}) = W_{F_{iA}}\dot{F}_{iA} + \frac{E}{2}(F_{jC}F_{jD}D_CD_D - 1)(F_{iB}D_BD_A)\dot{F}_{iA} + Cg_iD_AD_B\dot{G}_{iAB}. \tag{20}$$

3. Equilibrium

The derivation of the Euler equation and boundary conditions arising in second-gradient elasticity is well studied (Toupin, 1964), (Koiter, 1964), (Mindlin and Tiersten, 1962b) and (Germain, 2015). We reformulate the results in the present context for the sake of completeness and, in particular, for the purpose of establishing the connections between the applied loads and the deformations. The weak form of the equilibrium equations is given by the virtual-work statement

$$\dot{E} = P, \tag{21a}$$

where P is the virtual power of the applied loads, the superposed dot refers to the variational and/or Gateâux derivative and

$$E = \int_\Omega W(\mathbf{F},\varepsilon,\mathbf{g})dA \tag{22a}$$

is the strain energy.

In general, volumetric changes in materials' deformations are energetically expensive processes and thus are typically constrained in the constitutive modeling of engineering materials (see, Ogden, 1984; Steigmann, 2017). To accommodate the condition of the bulk incompressibility, the strain energy potential is augmented by the weak form, $p(J-1)$ as

$$U = W - p(J-1) \text{ and } E = \int_\Omega U(\mathbf{F},\varepsilon,\mathbf{g})dA, \tag{23}$$

where J is determinant of $\mathbf{F}$ and p is a constitutively indeterminate scalar field. The associated variation is then obtained by

$$\dot{U} = \dot{W} - p\dot{J}, \text{ and } \dot{J} = J_{\mathbf{F}}\mathbf{F}\cdot\dot{\mathbf{F}} = \mathbf{F}^*\cdot\dot{\mathbf{F}}. \tag{24}$$

Since the conservative loads are characterized by the existence of a potential L such that $P = \dot{L}$, the problem of determining equilibrium deformations is reduced to the problem of minimizing the potential energy, $E - L$. In the present case, this means

$$\dot{E} = \int_\Omega \dot{U}(\mathbf{F},\varepsilon,\mathbf{g},p)dA. \tag{25}$$

Now, we substitute Eqs. (21a) and (24) into Eq. (25) and thereby obtain

$$\dot{E} = \int_\Omega [W_{F_{iA}}u_{i,A} + \frac{E}{2}(F_{jC}F_{jD}D_CD_D - 1)(F_{iB}D_BD_A)u_{i,A} + C(g_iD_AD_B)u_{i,AB} - pF^*_{iA}u_{iA}]dA, \tag{26}$$

where $u_i = \dot{\chi}_i$ is the variation of the position field. Further, applying integration by part on $C(g_iD_AD_BG)u_{i,AB}$ yields

$$C(g_iD_AD_B)u_{i,AB} = C(g_iD_AD_Bu_{i,A})_{,B} - C(g_iD_AD_B)_{,B}u_{i,A}. \tag{27}$$

Thus Eqs. (26) and (27) furnish

$$\dot{E} = \int_{\Omega} [\{W_{F_{iA}} + \frac{E}{2}(F_{jC}F_{jD}D_CD_D - 1)(F_{iB}D_BD_A) - pF^*_{iA} - C(g_iD_AD_B)_{,B}\}u_{i,A} + C(g_iD_AD_Bu_{i,A})_{,B}]dA. \quad (28)$$

The above may be further reduced to

$$\dot{E} = \int_{\Omega} [W_{F_{iA}} + \frac{E}{2}(F_{jC}F_{jD}D_CD_D - 1)(F_{iB}D_BD_A) - pF^*_{iA} - C(g_iD_AD_B)_{,B}]u_{i,A}dA + \int_{\partial\Omega} C(g_iD_AD_Bu_{i,A})N_BdS, \quad (29)$$

where N_A is the rightward unit normal to $\partial\Omega$ in the sense of Green–Stokes theorem.

Consequently, we find

$$\dot{E} = \int_{\Omega} P_{iA}u_{i,A}dA + \int_{\partial\Omega} C(g_iD_AD_Bu_{i,A})N_BdS, \quad (30)$$

where

$$P_{iA} = W_{F_{iA}} + \frac{E}{2}(F_{jC}F_{jD}D_CD_D - 1)(F_{iB}D_BD_A) - pF^*_{iA} - C(g_iD_AD_B)_{,B} \quad (31)$$

is the expression of the Piola type stress. Also, for initially straight fibers (see, Eqs. (4) and (5)), the above further reduces to

$$P_{iA} = W_{F_{iA}} + \frac{E}{2}(F_{jC}F_{jD}D_CD_D - 1)(F_{iB}D_BD_A) - pF^*_{iA} - Cg_{i,B}D_AD_B. \quad (32)$$

Thus the Euler equation is obtained by

$$P_{iA,A} = 0 \text{ or } Div(\mathbf{P}) = \mathbf{0}, \quad (33)$$

which holds in Ω.

4. Boundary conditions

Applying integration by part on Eq. (30)(i.e. $P_{iA}u_{i,A} = (P_{iA}u_i)_{,A} - (P_{iA})_{,A}u_i$) furnishes

$$\dot{E} = \int_{\Omega} [(P_{iA}u_i)_{,A} - P_{iA,A}u_i]dA \int_{\partial\Omega} C(g_iD_AD_Bu_{i,A})N_BdS. \quad (34)$$

We then recast Eq. (34) by using Green-Stokes theorem as

$$\dot{E} = \int_{\partial\Omega} [P_{iA}u_iN_A + C(g_iD_AD_Bu_{i,A})N_B]dS - \int_{\Omega} P_{iA,A}u_idA. \quad (35)$$

Since the Euler equation ($P_{iA,A} = 0$) satisfied on Ω, the above reduces to

$$\dot{E} = \int_{\partial\Omega} P_{iA}u_iN_AdS + \int_{\partial\Omega} C(g_iD_AD_Bu_{i,A})N_BdS. \quad (36)$$

Now, we project $\nabla\mathbf{u}$ onto the normal and tangent directions and obtain

$$\nabla\mathbf{u} = \nabla\mathbf{u}(\mathbf{T}\otimes\mathbf{T}) + \nabla\mathbf{u}(\mathbf{N}\otimes\mathbf{N}) = \mathbf{u}'\otimes\mathbf{T} + \mathbf{u}_{,\mathbf{N}}\otimes\mathbf{N}, \quad (37)$$

where $\mathbf{T} = \mathbf{X}'(s) = \mathbf{k}\times\mathbf{N}$ is the unit tangent to the boundary $\partial\Omega$, and $\mathbf{u}'$ and $\mathbf{u}_{,N}$ are the tangential and normal derivatives of $\mathbf{u}$ on $\partial\Omega$ (i.e. $u_i' = u_{i,A}T_A$, $u_{i,N} = u_{i,A}N_A$). Thus, Eq. (36) can be decomposed into

$$\dot{E} = \int_{\partial\Omega} P_{iA}u_iN_AdS + \int_{\partial\Omega} Cg_iD_AD_B\left(u_i'T_AN_B + u_{i,N}N_AN_B\right)dS. \quad (38)$$

Also, using the following identity

$$Cg_iD_AD_BT_AN_Bu_i' = (Cg_iD_AD_BT_AN_Bu_i)' - (Cg_iD_AD_BT_AN_B)'u_i, \quad (39)$$

Eq. (38) becomes

$$\dot{E} = \int_{\partial\Omega} [P_{iA}N_A - (Cg_iD_AD_BT_AN_B)']u_idS + \int_{\partial\Omega} Cg_iD_AD_Bu_{i,N}N_AN_BdS + \int_{\partial\Omega} (Cg_iD_AD_BT_AN_Bu_i)'dS. \quad (40)$$

We then rewrite the above into the standard form:

$$\dot{E} = \int_{\partial\Omega} [P_{iA}N_A - (Cg_iD_AT_AD_BN_B)']u_idS + \int_{\partial\Omega} Cg_iD_AN_AD_BN_Bu_{i,N}dS - \sum \|Cg_iD_AT_AD_BN_Bu_i\|, \quad (41)$$

where the double bar symbol refers to the jump across the discontinuities on the boundary $\partial\Omega$ (i.e. $\|*\| = (*)^+ - (*)^-$) and the sum refers to the collection of all discontinuities.

It follows from (21a) that admissible powers are of the form

$$P = \int_{\partial w_t} t_iu_idS + \int_{\partial w} m_iu_{i,N}dS + \sum f_iu_i. \quad (42)$$

Hence, by comparing (41) and (42), we obtain

$$t_i = P_{iA}N_A - \frac{d}{dS}[Cg_iD_AT_AD_BN_B],$$
$$m_i = Cg_iD_AN_AD_BN_B,$$
$$f_i = Cg_iD_AT_AD_BN_Bu_i, \quad (43)$$

which are the expressions of edge tractions, edge moments and the corner forces, respectively.

For example, if the fiber's directions are either normal or tangential to the boundary (i.e. $(\mathbf{D}\cdot\mathbf{T})(\mathbf{D}\cdot\mathbf{N}) = 0$), (43) furnishes

$$t_i = P_{iA}N_A,$$
$$m_i = Cg_iD_AN_AD_BN_B,$$
$$f_i = 0, \quad (44)$$

where

$$P_{iA} = W_{F_{iA}} + \frac{E}{2}(F_{jC}F_{jD}D_CD_D - 1)(F_{iB}D_BD_A) - pF^*_{iA} - Cg_{i,B}D_AD_B,$$
$$g_{i,B} = F_{iC,BD}D_CD_D \text{(see, Eq. (5))}. \quad (45)$$

Thus, the solution of Eq. (33) can be uniquely determined by imposing the admissible set of boundary conditions in Eq. (43).

5. Hyperelastic matrix material – fiber composites

Based on the constitutive framework addressed in the previous sections, we develop a continuum-based prediction model which describes the responses of hyperelastic matrix material - fiber composites such as carbon-fiber-reinforced polymers and elastomeric composites. For this purpose, we employ the Mooney Rivlin strain energy potential, which is widely adopted in large deformation analyses (see, also, Ogden, 1984; Steigmann, 2017):

$$\widehat{W}(\mathbf{F}) = \frac{\mu}{2}(I_1 - 3) + \frac{\lambda}{2}(I_2 - 3), \quad (46)$$

where I_1 and I_2 are the principal invariants of the deformation gradient tensor which are given, respectively, by

$$I_1 = tr(\mathbf{F}^T\mathbf{F}) \text{ and } I_2 = \frac{1}{2}[(tr(\mathbf{F}^T\mathbf{F}))^2 - tr((\mathbf{F}^T\mathbf{F})^2)]. \quad (47)$$

Since $(I_1)_{\mathbf{F}} = 2\mathbf{F}$ and $(I_2)_{\mathbf{F}} = 2\mathbf{F}(I_1\mathbf{I} - \mathbf{F}^T\mathbf{F})$ (see, Steigmann, 2002), the variational derivative of Eq. (46) can be evaluated as

$$W_{\mathbf{F}}\cdot\dot{\mathbf{F}} = [\frac{\mu}{2}(I_1)_{\mathbf{F}} + \frac{\lambda}{2}(I_2)_{\mathbf{F}}]\cdot\dot{\mathbf{F}} = [\mu\mathbf{F} + \lambda\mathbf{F}\{(\mathbf{F}\cdot\mathbf{F})\mathbf{I} - \mathbf{F}^T\mathbf{F}\}]\cdot\dot{\mathbf{F}}. \quad (48)$$

Therefore, substituting Eq. (48) into Eq. (32), we obtain

$$\mathbf{P} = P_{iA}(\mathbf{e}_i\otimes\mathbf{E}_A) = [\mu F_{iA} + \lambda F_{iB}(F_{jC}F_{jC}\delta_{AB} - F_{jA}F_{jB}) + \frac{1}{2}E(F_{iB}F_{jC}F_{jC})D_AD_BD_DD_D - \frac{1}{2}EF_{iB}D_AD_B - Cg_{i,B}D_AD_B - pF^*_{iA}](\mathbf{e}_i\otimes\mathbf{E}_A), \quad (49)$$

which may serve as the expression of the Piola stress for hyperelastic composite materials. Further, the corresponding Euler equilibrium equation can be derived as

$$\begin{aligned}\mathbf{0} = Div(\mathbf{P}) = P_{iA,A}\mathbf{e}_i = [&\mu F_{iA,A}+\lambda\{F_{iB}(F_{jC}F_{jC}\delta_{AB}-F_{jA}F_{jB})\}_{,A}\\ &-Cg_{i,AB}D_AD_B - p_{,A}F^*_{iA} + \frac{1}{2}E(F_{iB}F_{jC}F_{jC})_{,A}D_AD_BD_DD_D\\ &-\frac{1}{2}EF_{iB,A}D_AD_B]\mathbf{e}_i,\end{aligned} \tag{50}$$

which hold on Ω.

In the above, μ and λ are the material constants of a hyperelastic matrix material of Mooney Rivlin type, and E and C are, respectively, the extension and bending modulus of fibers. For example, if the hyperelastic matrix material is reinforced with a single family of fibers (i.e. $\mathbf{D} = \mathbf{E}_1,\ D_1 = 1,\ D_2 = 0$) with the modulus of E and C, Eq. (50) furnishes

$$\begin{aligned}\mathbf{0} = \Big[&\mu\chi_{i,AA} - p_{,A}\varepsilon_{ij}\varepsilon_{AB}\chi_{j,B}+\lambda(\chi_{i,AA}\chi_{j,C}\chi_{j,C} + \chi_{i,A}\chi_{j,CA}\chi_{j,C}\\ &+ \chi_{i,A}\chi_{j,C}\chi_{j,CA}-\chi_{i,BA}\chi_{j,A}\chi_{j,B} - \chi_{i,B}\chi_{j,A}\chi_{j,AB} - \chi_{i,B}\chi_{j,A}\chi_{j,BA})\\ &+\frac{1}{2}E(\chi_{i,11}\chi_{j,1}\chi_{j,1} + \chi_{i,1}\chi_{j,11}\chi_{j,1} + \chi_{i,1}\chi_{j,1}\chi_{j,11})\\ &-\frac{1}{2}EF_{i1,1} - C\chi_{i,1111}\Big]\mathbf{e}_i,\end{aligned} \tag{51}$$

where $F_{iA} = \chi_{i,A} = \frac{\partial\chi_i}{\partial X_A}$, $F^*_{iA} = \varepsilon_{ij}\varepsilon_{AB}F_{jB}$, and ε_{ij} is the 2-D permutation; $\varepsilon_{12} = -\varepsilon_{21} = 1, \varepsilon_{11} = -\varepsilon_{22} = 0$. Performing Einstein summation and with some effort, we arrive at

$$\begin{aligned}0 = &\mu(\chi_{1,11} + \chi_{1,22}) - p_{,1}\chi_{2,2} + p_{,2}\chi_{2,1}+\lambda(\chi_{1,11}\chi_{2,2}\chi_{2,2}\\ &+ \chi_{1,22}\chi_{2,1}\chi_{2,1} + 2\chi_{1,1}\chi_{2,21}\chi_{2,2} + 2\chi_{1,2}\chi_{2,12}\chi_{2,1}\\ &- \chi_{1,21}\chi_{2,1}\chi_{2,2} - \chi_{1,12}\chi_{2,2}\chi_{2,1} - \chi_{1,2}\chi_{2,11}\chi_{2,2}\\ &- \chi_{1,1}\chi_{2,22}\chi_{2,1} - \chi_{1,2}\chi_{2,1}\chi_{2,21} - \chi_{1,1}\chi_{2,2}\chi_{2,12})\\ &+\frac{1}{2}E(3\chi_{1,11}\chi_{1,1}\chi_{1,1} + \chi_{1,11}\chi_{2,1}\chi_{2,1}\\ &+2\chi_{2,11}\chi_{1,1}\chi_{2,1}) - C\chi_{1,1111},\end{aligned} \tag{52}$$

$$\begin{aligned}0 = &\mu(\chi_{2,11} + \chi_{2,22}) - p_{,2}\chi_{1,1} + p_{,1}\chi_{1,2}+\lambda(\chi_{2,11}\chi_{1,2}\chi_{1,2}\\ &+ \chi_{2,22}\chi_{1,1}\chi_{1,1} + 2\chi_{2,1}\chi_{1,21}\chi_{1,2} + 2\chi_{2,2}\chi_{1,12}\chi_{1,1}\\ &- \chi_{2,21}\chi_{1,1}\chi_{1,2} - \chi_{2,12}\chi_{1,2}\chi_{1,1} - \chi_{2,2}\chi_{1,11}\chi_{1,2}\\ &- \chi_{2,1}\chi_{1,22}\chi_{1,1} - \chi_{2,2}\chi_{1,1}\chi_{1,21} - \chi_{2,1}\chi_{1,2}\chi_{1,12})\\ &+\frac{1}{2}E(3\chi_{2,11}\chi_{2,1}\chi_{2,1} + \chi_{2,11}\chi_{1,1}\chi_{1,1}\\ &+2\chi_{1,11}\chi_{2,1}\chi_{1,1}) - C\chi_{2,1111},\end{aligned} \tag{53}$$

which together with the constraint of the bulk incompressibility,

$$\det\mathbf{F} = \chi_{1,1}\chi_{2,2} - \chi_{1,2}\chi_{2,1} = 1, \tag{54}$$

solves the unknown potentials of χ_1, χ_2 and p. The solution of the above PDE can be uniquely determined by imposing the admissible boundary conditions in Eq. (44). For the rectangular shaped samples where $\mathbf{D}\cdot\mathbf{T} = 0$ and $\mathbf{D}\cdot\mathbf{N} = 1$, Eq. (44) takes the following form

$$\begin{aligned}t_1 &= P_{11},\ t_2 = 0,\\ m_1 &= Cg_1,\ m_2 = 0,\\ f_1 &= f_2 = 0.\end{aligned} \tag{55}$$

In addition, from Eqs. (5) and (49), the expressions of P_{11} and g_1 can be obtained, respectively, as

$$\begin{aligned}P_{11} = &\mu\chi_{1,1}+\lambda(\chi_{1,1}\chi_{2,2}\chi_{2,2}-\chi_{1,2}\chi_{2,1}\chi_{2,2})\\ &+\frac{1}{2}E\chi_{1,1}(\chi_{1,1}\chi_{1,1} + \chi_{2,1}\chi_{2,1} + \chi_{1,2}\chi_{1,2} +_{2,1}\chi_{2,22,1}\chi_{2,2})\\ &-\frac{1}{2}E\chi_{1,1}-C\chi_{1,111} - p\chi_{2,2},\end{aligned}$$

$$g_1 = G_{111}D_1D_1 = \chi_{1,11}. \tag{56}$$

The numerical solution of the obtained PDE system (Eqs. (42)–(44)) can be accommodated via commercial packages (e.g. Matlab, COMSOL etc...). The details of numerical procedures are reserved in the " Appendix" for the sake of coherence.

5.1. Consideration of linear theory

Although the proposed model is intended for large deformation analyses, the development of the compatible linear model may be of practical interest especially when the induced deformations are determined to be '*small* '. In such cases, the linear theory may supply reasonable alternatives with reduced computational resources. Our intention here is to investigate the possibility of a compatible linear model for the materials of the Mooney Rivlin type within the description of superposed incremental deformations.

We consider superposed '*small*' deformations defined by

$$\chi = \chi_o + \epsilon\dot{\chi}\ ;\ |\epsilon| \ll 1, \tag{57}$$

where $(\dot{*}) = \partial(*)/\partial\varepsilon$, $\dot{\chi} = \mathbf{u}$ and $(*)_o$ denote configuration of $*$, evaluated at $\epsilon = 0$, $(\dot{*}) = \partial(*)/\partial\varepsilon$. Here caution needs to be taken that the present notation is not confused with the one used for the variational computation. Accordingly, the deformation gradient tensor can be approximated as

$$\mathbf{F} = \mathbf{F}_o + \epsilon\nabla\mathbf{u},\ \text{where}\ \dot{\mathbf{F}} = \nabla\mathbf{u}. \tag{58}$$

In a typical environment, the body is initially undeformed and stress free (i.e. at $\varepsilon = 0$, $\mathbf{F}_o = \mathbf{I}$ and $\mathbf{P}_o = \mathbf{0}$). To accommodate the initial conditions, we require

$$\mathbf{F}_o = \mathbf{I}\ \text{and}\ \mathbf{P}_o = \mathbf{0},\ \text{at}\ \varepsilon = 0, \tag{59}$$

from which Eq. (58) reduces to

$$\mathbf{F} = \mathbf{I} + \varepsilon\nabla\mathbf{u}, \tag{60}$$

and successively yields

$$\mathbf{F}^{-1} = \mathbf{I} - \epsilon\nabla\mathbf{u}+o(\epsilon)\ \text{and}\ J = \det\mathbf{F} = 1 + \epsilon\,\text{div}\mathbf{u}+o(\epsilon). \tag{61a}$$

Also, in view of Eq. (57), we approximate Eq. (33) as

$$Div(\mathbf{P}) = Div(\mathbf{P}_o) + \epsilon Div(\dot{\mathbf{P}}) + o(\epsilon) = \mathbf{0}. \tag{62}$$

Dividing the above by ϵ and letting $\epsilon \to 0$, we find the following linearized Euler equation

$$Div(\dot{\mathbf{P}}) = \mathbf{0}\ \text{or}\ \dot{P}_{iA,A} = 0, \tag{63}$$

where the expression of $\dot{P}_{iA}$ can be obtained from Eq. (45) that

$$\begin{aligned}\dot{P}_{iA} = &(W_{F_{iA}})^{\cdot} + E[\dot{F}_{jC}(F_{jD})_oD_CD_D][(F_{iB})_oD_BD_A)]\\ &+\frac{E}{2}[(F_{jC})_o(F_{jD})_oD_CD_D - 1](\dot{F}_{iB}D_BD_A) - \dot{p}(F^*_{iA})_o\\ &- p\dot{F}^*_{iA} - \dot{g}_{i,B}D_AD_B.\end{aligned} \tag{64}$$

Since $(F_{jD})_o = \delta_{jD}$ and $(F^*_{iA})_o = \delta_{iA}$ at $\epsilon = 0$, Eq. (64) further reduces to

$$\dot{P}_{iA} = (W_{F_{iA}})^{\cdot} + Eu_{j,B}D_AD_BD_iD_j - \dot{p}\delta_{iA} - p\dot{F}^*_{iA} - u_{i,BCD}D_CD_DD_AD_B, \tag{65}$$

where $\delta_{jC}\delta_{jD}D_CD_D = D_CD_C = 1$ and $\dot{g}_{i,B} = \dot{F}_{iC,BD}D_CD_D$. We note that, in the above equation, the initial director field $\mathbf{D}$ is represented by the current basis (i.e. $D_i\mathbf{e}_i$) not by the reference frame (i.e. $D_A\mathbf{E}_A$). This is due to the collapse of two different bases arising in linear elasticity theory (i.e. $\mathbf{e}_i \equiv \mathbf{E}_A$; see, also, Ogden, 1984; Steigmann, 2017). Hence, the associated tensor operations are possible without conflicting the bases.

Now we find from Eqs. (48) and (49) that

$$(W_{F_{iA}})^{\cdot} = \mu\dot{F}_{iA} + \lambda\dot{F}_{iB}(\delta_{jC}\delta_{jC}\delta_{AB} - \delta_{jA}\delta_{jB})$$

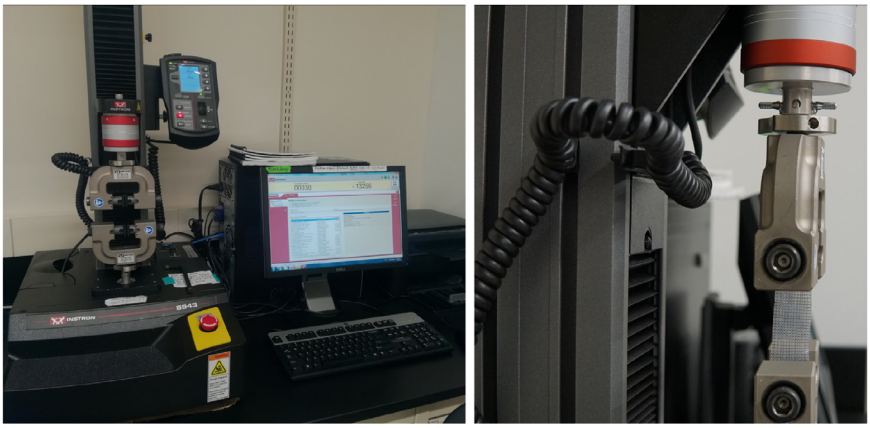

Fig. 1. Experimental set up: Elastomeric composite sample (50mm × 25mm) under uniaxial tension test.

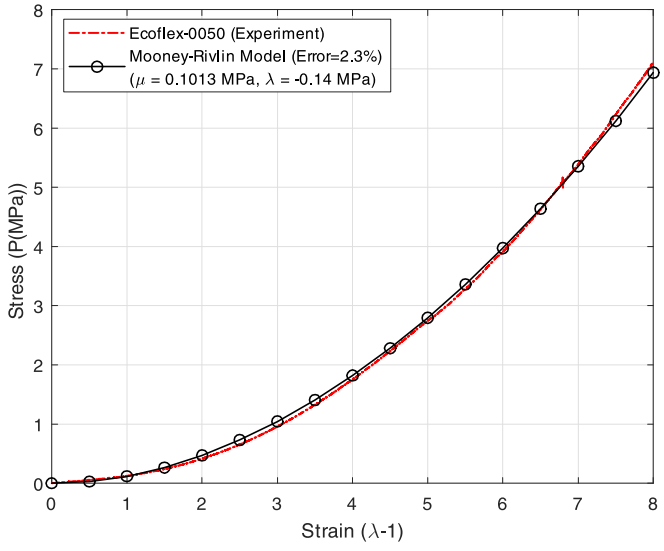

Fig. 2. Stress-strain curves: Ecoflex-0050 and the Mooney Rivlin curve fitting.

$$+\lambda\delta_{iB}(2\dot{F}_{jC}\delta_{jC}\delta_{AB}-\dot{F}_{jA}\delta_{jB}-\delta_{jA}\dot{F}_{jB})$$
$$=\mu\dot{F}_{iA}+2\lambda\dot{F}_{BB}\delta_{iA}-\lambda\dot{F}_{Ai}, \tag{66}$$

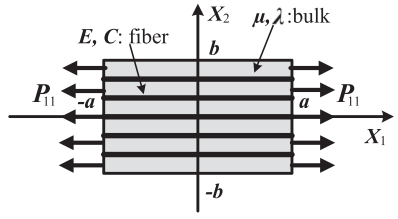

Fig. 4. Schematic of the problem: $2a = 50$ mm and $2b = 25$ mm.

which may serve as the linearized variational form of the Mooney Rivlin strain energy potential. The substitution of Eq. (66) into Eq. (64) then furnishes

$$\dot{P}_{iA}=\mu u_{i,A}-\lambda u_{A,i}+Eu_{j,B}D_AD_BD_iD_j-\dot{p}\delta_{iA}-p_o\dot{F}^*_{iA}$$
$$-u_{i,BCD}D_CD_DD_AD_B, \tag{67}$$

where $p_o=\mu$ to recover the initial stress free state at $\epsilon=0$ (i.e. $(\dot{P}_{iA})_{\epsilon=0}=0$), and $\dot{F}_{BB}=u_{B,B}$ vanishes from the linearized condition of bulk incompressibility; i.e.,

$$(J-1)^{\cdot}=(F^*_{iA})_o\,\dot{F}_{iA}=\delta_{iA}u_{i,A}=u_{A,A}=0. \tag{68}$$

In addition, using the identities of $\dot{F}^*_{iA,A}=0$ (Piola's identity) and $(\dot{p}\delta_{iA})_{,A}=\dot{p}_{,A}\delta_{iA}=\dot{p}_{,i}$, the expression of $\dot{P}_{iA,A}$ can be formulated as

$$\dot{P}_{iA,A}=\mu u_{i,AA}-\lambda u_{A,iA}+Eu_{j,AB}D_AD_BD_iD_j-\dot{p}_{,i}$$

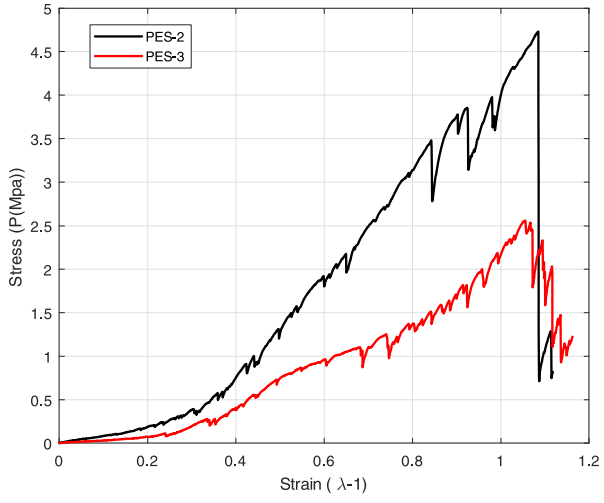

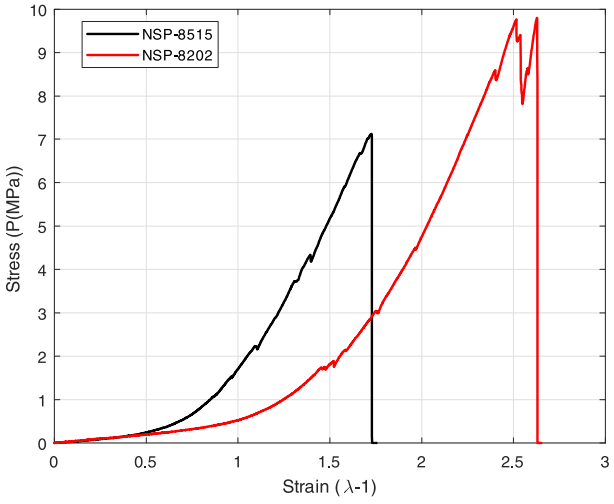

Fig. 3. (a) Stress-strain: PES-2 and PES-3 fibers. (b) Stress-strain: NSP-8515 and NSP-8020 fibers.

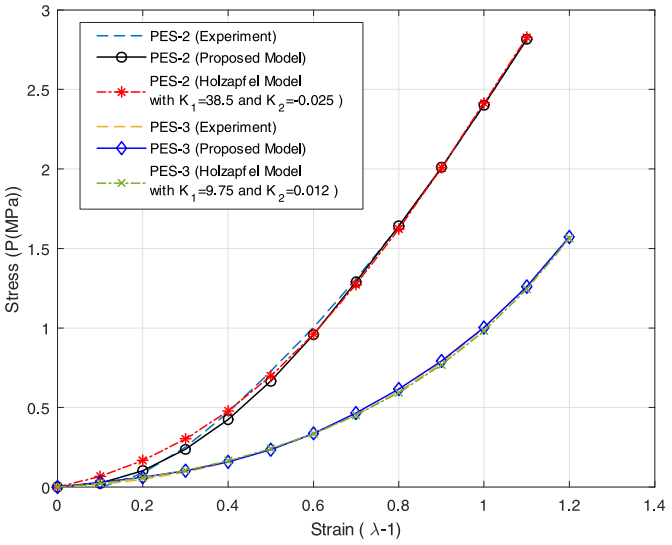

Fig. 5. Stress-strain curves from different prediction models: PES-2 & PES-3.

$$-u_{i,ABCD}D_C D_D D_A D_B = 0. \tag{69}$$

But, from the compatibility condition of $u_{A,iA}$, together with Eq. (68), it is not difficult to show

$$u_{A,iA} = u_{A,Ai} = (u_{A,A})_i = 0. \tag{70}$$

Consequently, Eq. (69) becomes

$$\dot{P}_{iA,A} = \mu u_{i,AA} + E u_{j,AB} D_A D_B D_i D_j - \dot{p}_{,i} - u_{i,ABCD} D_C D_D D_A D_B = 0, \tag{71}$$

which can serve as the compatible linear Euler equation for the materials of Mooney Rivlin type.

We remark that the linearized equations derived from the proposed model (Eq. (71)) are the same as those obtained from the setting of the Neo Hookean based model (see, Eq. (56) in Zeidi and Kim, 2017b or Eq. (77) in Kim and Zeidi, 2018). This is mainly due to the fact that the influence of the higher-order invariant term, I_2, in the Mooney Rivlin energy potential is gradually diminished as it enters into the small deformation regime. Since the existence of the high-order invariant term I_2 is the primary distinction between the Mooney Rivlin and Neo Hookean models, the above result would mean that the two models become essentially identical within the prescription of superposed incremental deformations. Therefore, the linear consideration of the Mooney Rivlin potential may not be necessary in the present case. The corresponding solutions of Eqs. (68) and (71) and the necessary boundary conditions can be found in Zeidi and Kim (2017b) and Kim and Zeidi (2018).

6. Model implementation and discussions

A comparison with experimental results is presented in this section to demonstrate the performance and utility of the proposed model. We designed the uniaxial tension test of four different types of elastomeric composites that are reinforced, respectively, by polyester/spandex fibers (PES-2, PES-3) and nylon/spandex fibers (NSP-8515, NSP-8020). *Ecoflex 0050* (Smooth-on Inc., USA) is used for the matrix materials for all the fiber samples, which is known to be one of the promising materials in biomechanical applications for its high tear resistance and large extensibility. The reinforced elastomeric composites were fabricated in a three-layer configuration using the layer by layer method. First, *Ecoflex 0050* elastomer was prepared by mixing two components (a base and curing agent) in 1: 1 ratio and subsequently degassed in a vacuum chamber to remove entrapped bubbles. The second layer of long fibers was then placed flat on the elastomer and allowed to wet at the interface. A small amount of elastomer was poured and rolled over the fibers to wet it again and to fill the gaps between pores and level the second layer. Lastly, a sufficient amount of elastomer was poured over the second layer and placed into the film applicator rod to yield uniform film. The dimensions of the fabricated elastomeric composites were measured using a caliper and an aspect ratio of length-to-width of 2: 1 was maintained for all samples. Instron 5943 (Illinois Tool Works Inc., USA) was used to measure stress-strain responses of the prepared composites (See Fig. 1). The extension rate was set to be $10mm$ per minute to avoid/minimize viscous responses. The stress-strain curves and the deformations of material points on the samples were simultaneously recorded for the purpose of comparisons with the theoretical predictions obtained from the proposed model.

The material parameters of the matrix material (i.e. λ and μ) are determined from the stress-strain curve of Ecoflex-0050 (see, Fig. 2) using the Mooney-Rivlin model. The elastic modulus of fibers (i.e. E and C) are obtained from the stress-strain curves of the four different fibers (Fig. 3(a) and (b)) in which we used the formula (Mihai and Goriely, 2017)

$$E = \frac{P}{a - \lambda(a)}(1 - \lambda'(a)) \tag{72}$$

Here, P and a are the stress and extension ratio of fibers, respectively, while $\lambda(a)$ is the stretch ratio in the orthogonal direction

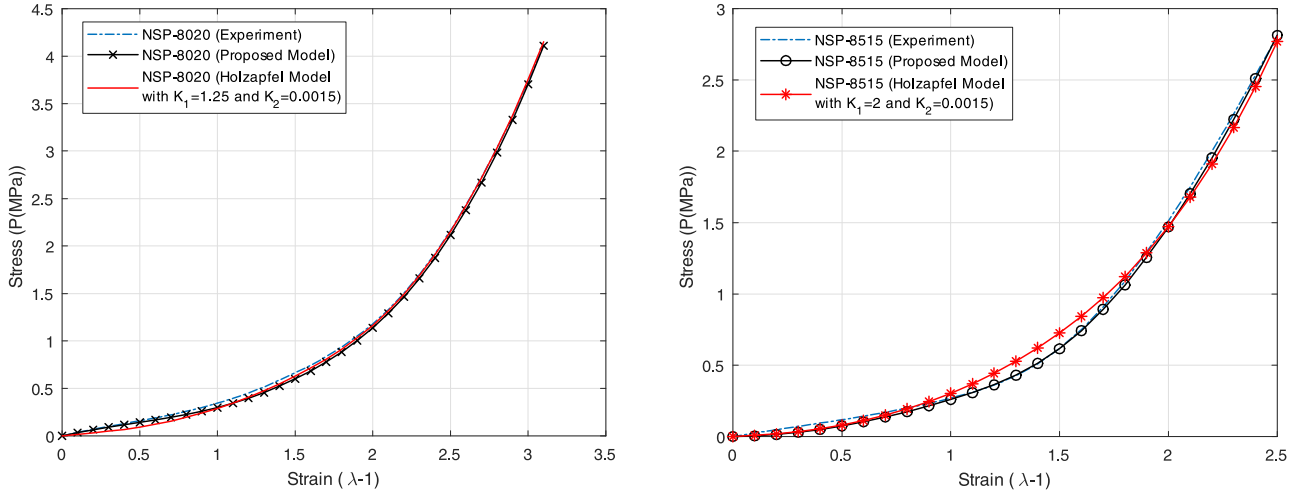

Fig. 6. Stress-strain curves from different prediction models: PES-2 & PES-3: NSP8020-2 & NSP8515.

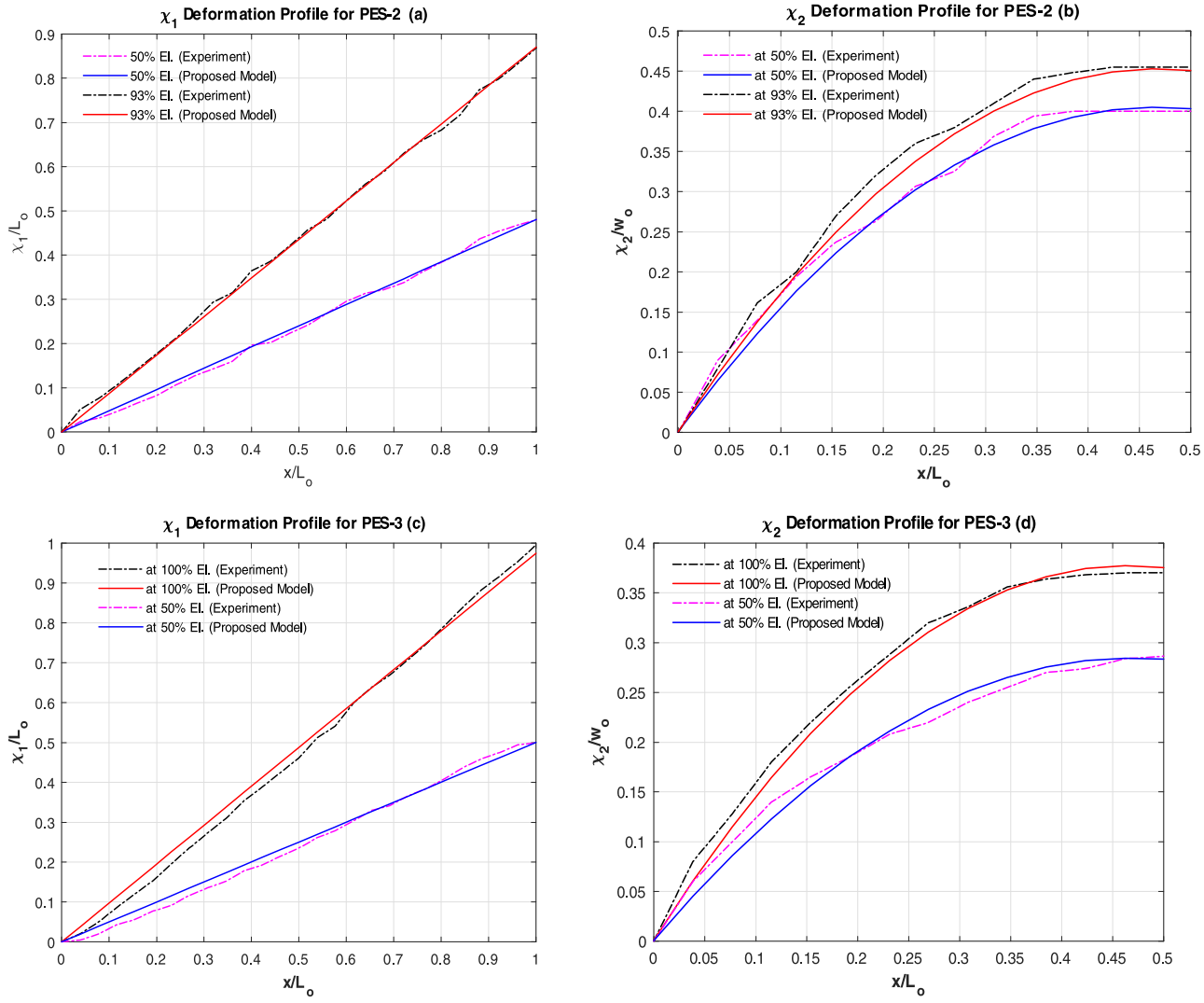

Fig. 7. Deformation profiles: (a) χ_1 (PES-2); (b) χ (PES-2); (c) χ_1 (PES-3); (d) χ_2(PES-3).

from the stress-strain data of fibers (Fig. 3(a) and (b)). The obtained material properties are then used as the input parameters of the PDEs in Eqs. (64) and (65), which are numerically solved via the custom-built algorithm (see, Appendix). In the assimilations, the applied load P_{11} is computed from Eq. (49) such that

$$\begin{aligned} P_{11} &= \mu\chi_{1,1}+\lambda(\chi_{1,1}\chi_{2,2}\chi_{2,2}-\chi_{1,2}\chi_{2,1}\chi_{2,2}) \\ &\quad + \frac{1}{2}E\chi_{1,1}(\chi_{1,1}\chi_{1,1} + \chi_{2,1}\chi_{2,1} + \chi_{1,2}\chi_{1,2} + {}_{2,1}\,\chi_{2,22,1}\chi_{2,2}) \\ &\quad - \frac{1}{2}E\chi_{1,1} - C\chi_{1,111} - p\chi_{2,2}. \end{aligned} \tag{73}$$

The associated boundary conditions are prescribed as follows (see, Fig. 4.):

$$\begin{aligned} &t_1 = P_{11},\ t_2 = P_{12} = 0,\ \text{at } X_1 = a, -a \text{ and} \\ &t_1 = P_{21} = 0,\ t_2 = P_{22} = 0,\ \text{at } X_2 = b, -b. \end{aligned} \tag{74}$$

In addition, the following Holzapfel model (Holzapfel et al., 2000) is used in the estimation of the experimental results:

$$W = \frac{c}{2}(I_1 - 3) + \frac{k_1}{2k_2}\sum_{i=4,6}\{\exp[k_2(I_i - 1)^2] - 1\}, \tag{75}$$

where c is the property of matrix and k_1 and k_2 are empirical fitting parameters pertaining to the composites. The obtained results are then compared with the predictions made by the proposed model. The Holzapfel model is widely adopted in biomaterials applications such as mimicking natural aorta, vein, cartilage and aortic valve where the *J-shaped* stress-strain responses (see, Fung, 1984; Vatankhah-Varnosfaderani et al., 2017; Yan et al., 2017 and Zhalmuratova et al.) and significant anisotropy (Fung, 1993; Abe and Hayashi, 1996) are the primary design considerations. Our intention for the model comparison is to investigate the potential applications of the proposed model in the design and analysis of biomimetic materials that can be implanted to replace or repair damaged/missing tissue.

A comparison among the stress-strain curves obtained from the experimental data, the proposed model and the Holzapfel model are presented in Figs. 5 and 6. It is shown in Figs. 5 and 6 that the proposed model successfully predict the *J-shaped* stress-strain responses of the composites regardless of the different strain- stiffening rates. The Holzapfel model also produces reasonably accurate estimations of the stress-strain curves of the tested samples except the slight deviations in the transition (i.e. strain-stiffening) regimes of PES-3 and NSP-8515 composites where rapid strain-stiffening responses are observed at a low strain level. In other words, the Holzapfel model is less sensitive to the steep variations of the stress-strain curve than the proposed model. Such limited sensitivity may not compromise the overall prediction accuracy of the model. However, it may be potential disadvantage, especially

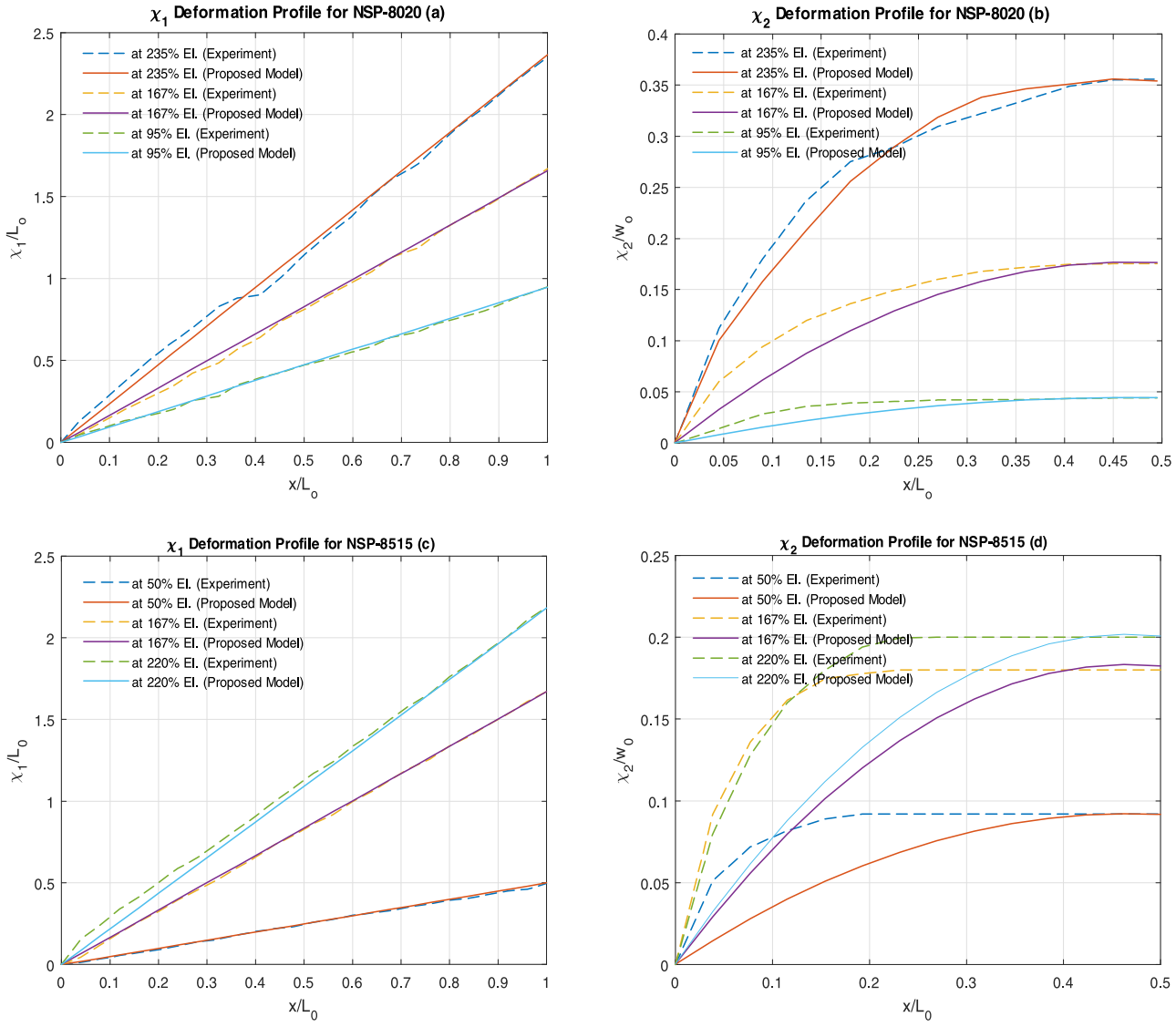

Fig. 8. Deformation profiles: (a) χ_1 (NSP-8020); (b) χ_2 (NSP-8020); (c) χ_1(NSP-8515); (d) χ_2 (NSP-8515).

when mimicking biological tissues, considering the fact that one of the primary requirements of the theoretical model is the ability to predict rapid strain-stiffening behaviors at a low level of strain, which is also known to be a characteristic of most biological tissues (Fung, 1984; Vatankhah-Varnosfaderani et al., 2017).

More importantly, unlike the Holzapfel model in which the empirical constants k_1 and k_2 are obtained from the fabricated composites, the proposed model predicts the resultant properties of desired composites prior to the composition as long as the material parameters of matrix materials and fibers are provided (i.e. no empirical curve fitting of the composite is necessary). This may be of more practical interest, especially in the design stage of composites. Since the responses of the intended composites can be predetermined using the proposed model, through which the required resources in the sample productions may be minimized.

In addition to the abovementioned technical merits, the proposed model provides the quantitative predictions of other key design considerations such as deformation profiles and contours, and shear strain distributions. Fig. 7(a)–(d) illustrate the χ_1 and χ_2 deformation profiles of the polyester/spandex fiber-composites (PES-2, PES-3) at different strain levels. Despite the inevitable uncertainties (e.g. image processing and curve fitting), the deformation profiles from the experiment and the theoretical predictions demonstrate close agreement throughout the entire domain of interest. In the case of the nylon/spandex fiber-composites (NSP-8515, NSP-8020), the proposed model accurately predicts the χ_1 deformations (axial elongation) of both samples (see, Fig. 8(a)–(c)), yet has limitations in the prediction of χ_2 deformations, especially those in the NSP-8515 composites at lower strain levels (Fig. 8(d)). This may be due to the NSP-8515 fibers' resistance along the χ_2 direction within the composites, which hinders the χ_2 deformation. We speculate that the bidirectional fiber model may be suitable for the deformation analysis of NSP-8515 fiber-composites. Further research on these cases is, however, beyond the scope of the present study, yet is certainly of practical interest. The graphical comparisons between the theoretical prediction and experimental result for the cases of the PES-3 sample at 50% and 100% elongations, and the NSP-8020 sample at 167% and 235% elongations are presented in Figs. 9-10 for the purpose of cross-examination with the deformation data obtained in Figs. 7 and 8. The plotted deformation contours are the norms of displacement fields (i.e.$\sqrt{\chi_1^2+\chi_2^2}$) and demonstrate reasonably close agreement with the deformed configurations of both composite samples. The same comparisons are made for the PES-2 and NSP-8515 cases, which again indicate close

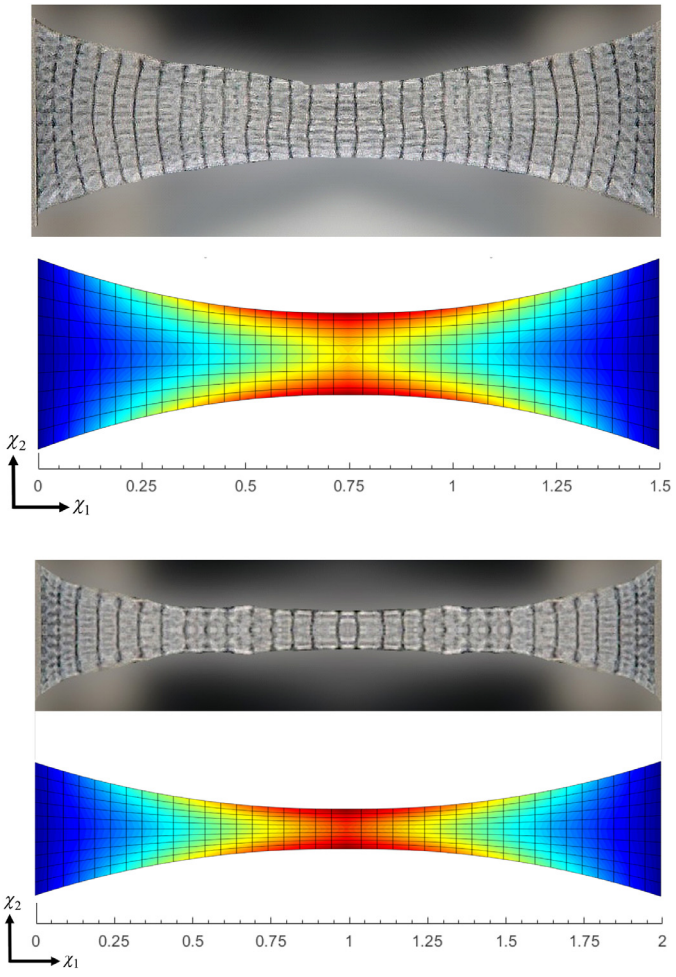

Fig. 9. Comparisons of the overall deformations: PES-3 at 50% (top) and 100% (bottom) elongations.

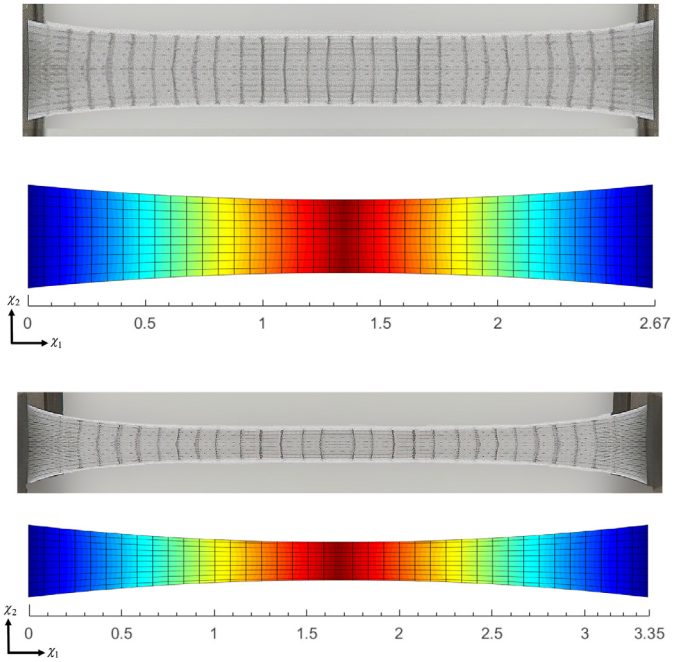

Fig. 10. Comparisons of the overall deformations: NSP-8020 at 167% (top) and 235% (bottom) elongations.

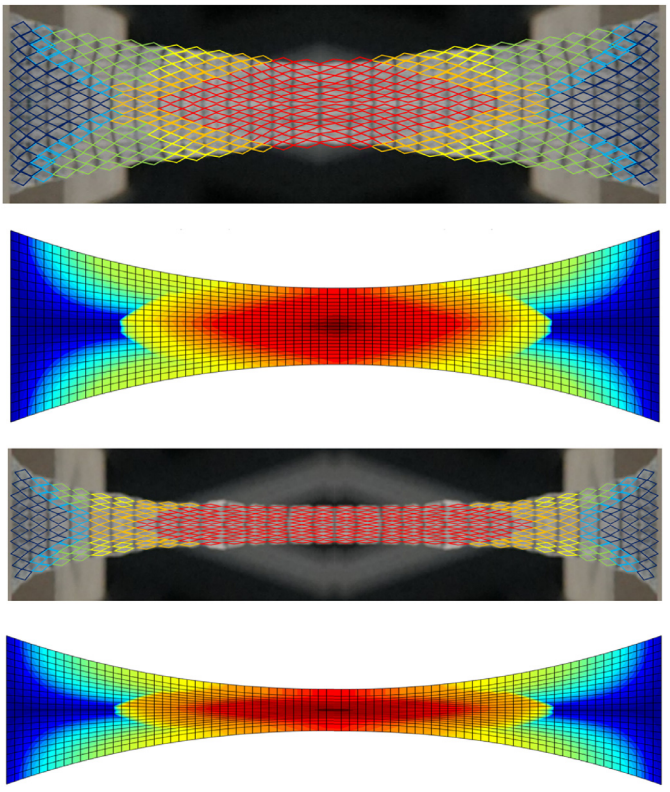

Fig. 11. Shear angle distributions: PES-3 at 50% (top) and 100% (bottom) elongation.

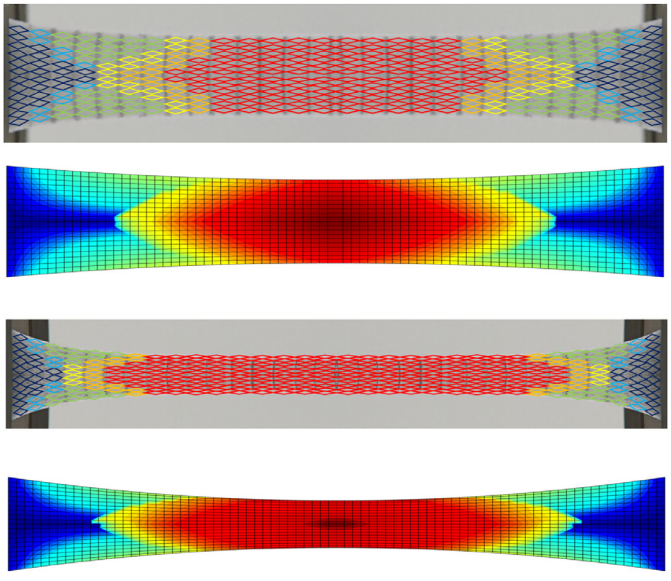

Fig. 12. Shear angle distributions: NSP8020 at 167% (top) and 235% (bottom) elongation.

correspondence with experiments except NSP-8515 at 50% elongation (see, also, Fig. 8(d)). However, these have been intentionally omitted for the sake of conciseness.

Lastly, the shear angle distributions from both the experiments and theoretical predictions are presented through Figs. 10 and 11. The corresponding shear angle configurations are mapped using a fine mesh grid of $1.78mm \times 1.78mm$ printed on the surfaces of the PES-3 and NSP-8020 composite samples. The deformed material points are measured from the intersections of printed mesh grids and subsequently processed via the Matlab image processing tool

in order to compute the shear strain relation of $\gamma_{xy} = \alpha + \beta$, where $\tan(\alpha) = \chi_{2,1}/(1 + \chi_{1,1})$ and $\tan(\beta) = \chi_{1,2}/(1 + \chi_{2,2})$. The prediction results in Figs. 10 and 11 clearly indicate that the obtained model successfully estimates the shear strain distributions of the PES-3 composite at 50% and 100%, and the NSP-8020 composite at 167% and 235% strain levels. In particular, the shear strain distributions predicted by the proposed model are smooth and continuous over the entire domain of interest unlike those depicted by the classical (first-order) continuum theory where significant discontinuities are present (see, also, Dell'Isola et al., 2017 and Dell'Isola et al., 2016a). Further, the corresponding stress fields become "Piola type double stress" (see, for example, Javili et al., 2013; dell'Isola et al., 2012; dell'Isola et al., 2016) due to the introduction of bending stiffness of fibers into the model of continuum deformation (second-gradient continuum). In other words, the resulting stress fields now depend both on the axial stiffness (E) and bending stiffness (C) of fibers (see, Eq. 73). More detailed discussions regarding the qualitive sensitivity of the deformation, stress and strain fields with respect to the material parameters of fibers can be found in Zeidi and Kim (2018, 2017b) and Kim and Zeidi (2018). In the present case, the J-shaped stress-strain response of a certain composite tends to be stiffer with increasing bending modulus of fibers. The result may be further extended to the failure analysis of highly strained fiber-elastomer composites by providing quantitative measurements of the shear strain energy distributions of the desired composites.

Overall, the proposed model successfully predicts the various important mechanical responses of the tested elastomeric composites and therefore may also serve as an alternative of the Holzapfel model in the design and analysis of biomimetic composites, especially those exhibiting significant strain-stiffening responses at a low level of strain.

7. Conclusion

In this study, we present a continuum model for the mechanics of a hyperelastic polymer material reinforced with polyester fibers in finite plane elastostatics. The reinforcing long fibers are idealized as continuously distributed spatial rods of the Kirchhoff type, where the elastic resistant of fibers against stretch and flexure are integrated into the models of the continuum deformation via the first and second gradient of deformations, respectively. We place an emphasis on the assimilation of *J-shaped* stress-strain behaviors of the elastomeric composites while maintaining the rigor and sufficient generality in the derivation of the associated constitutive formulation. To accommodate the hyperelastic responses of the matrix material (*Ecoflex 0050*), the strain energy function of the composite is refined by the Mooney Rivlin model. Within the framework of the second gradient theory, the Euler equation and necessary boundary conditions are also derived using the variational principles and the virtual work statement. These, in turn, furnishes a highly nonlinear PDE from which a set of numerical solutions describing the hyperelastic responses of the composites are obtained via the custom-built numerical procedures.

More importantly, we demonstrated that the presented model successfully predicts rapid strain-stiffening behavior of the *Ecoflex 00500-fiber* composite at low strain level. Further, the deformation profiles and shear angle distributions of the composites are computed which demonstrate good agreement with the in-house experiment and the existing results in literature. In particular, the obtained model directly predicts the resultant stress-strain responses of the composite via the integration of the known modulus of matrix materials and fibers. This may facilitate the design and analysis of a certain composite, since the model provides the instant estimations of the mechanical responses of composite prior to the fabrication. Potential applications may also include the failure analysis of highly strained elastomeric composites by estimating the shear strain fields from the obtained deformation map through which the corresponding shear energy distributions can be obtained. Lastly, we mention that the proposed model may serve as an alternative of the Holzapfel model in the estimations of rapid stress-strain responses of hyperelastic composite materials.

Declaration of Competing Interest

The authors declare that they have no known competing financial interests or personal relationships that could have appeared to influence the work reported in this paper.

Acknowledgments

This work was supported by the Natural Sciences and Engineering Research Council of Canada via Grant #RGPIN 04742. Kim would like to thank Dr. David Steigmann for stimulating his interest in this subject and for discussions concerning the underlying theory.

Appendix A. Finite element analysis of the 4th order coupled PDE

The systems of PDEs in Eqs. (52)–(54) are 4th order differential equations with coupled non-linear terms. The case of such less regular PDEs deserve delicate mathematical treatment and is of particular practical interest. Hence, it is not trivial to demonstrate the associated numerical analysis procedures.

For preprocessing, Eqs. (52)–(54) may be recast as

$$
\begin{aligned}
0 &= \mu(Q+\chi_{1,22}) - A\chi_{2,2} + B\chi_{2,1} - CQ_{,11} + \lambda(QFF + \chi_{1,22}DD + 2C\chi_{2,21}F + 2E\chi_{2,12}D - \chi_{1,21}DF - \chi_{1,12}FD \\
&\quad -ERF - C\chi_{2,22}D - ED\chi_{2,21} - CF\chi_{2,12}) - \frac{1}{2}EQ + \frac{1}{2}E(3Q\chi_{1,1}\chi_{1,1} + Q\chi_{2,1}\chi_{2,1} + 2R\chi_{1,1}\chi_{2,1}) \\
0 &= \mu(\chi R + \chi_{2,22}) - B\chi_{1,1} + A\chi_{1,2} - CR_{,11} + \lambda(REE + \chi_{2,22}CC + 2D\chi_{1,21}E + 2F\chi_{1,12}C - \chi_{2,21}CE - \chi_{2,12}EC \\
&\quad -FQE - D\chi_{1,22}C - FC\chi_{1,21} - DE\chi_{1,12}) - \frac{1}{2}ER + \frac{1}{2}E(3R\chi_{2,1}\chi_{2,1} + R\chi_{1,1}\chi_{1,1} + 2Q\chi_{2,1}\chi_{1,1}) \\
0 &= Q - \chi_{1,11}, \\
0 &= R - \chi_{2,11}, \\
0 &= C - \chi_{1,1}, \\
0 &= D - \chi_{2,1}, \\
0 &= E - \chi_{1,2}, \\
0 &= F - \chi_{2,2}, \\
0 &= A - \mu(Q+\chi_{1,22}) - CQ_{,11}, \\
0 &= B - \mu(R+\chi_{2,22}) - CR_{,11},
\end{aligned}
\tag{76}
$$

where $Q=\chi_{1,11}$, $R=\chi_{2,11}$, $C=\chi_{1,1}$, $D=\chi_{2,1}$, $E=\chi_{1,2}$, $F=\chi_{2,2}$. Thus, the order of differential equations is reduced from the three coupled equations of 4th order to ten coupled equations of 2nd order. In particular, the non-linear terms in the above equations (e.g. $A\chi_{2,2}$, $B\chi_{2,1}$ etc...) can be systematically treated via the following Picard iterative procedure:

$$
\begin{aligned}
&-A^{initial}\chi_{2,2}^{initial} + B^{initial}\chi_{2,1}^{initial} \;\Rightarrow\; -A_0\chi_{2,2}^{0} + B_0\chi_{2,1}^{0} \\
&\;A^{initial}\chi_{1,2}^{initial} - B^{initial}\chi_{1,1}^{initial} \Longrightarrow A_0\chi_{1,2}^{0} - B_0\chi_{1,1}^{0},
\end{aligned}
\tag{77}
$$

where the estimated values of A and B continue to be updated based on their previous estimations (e.g. A_1 and B_1 are refreshed by their previous pair of A_o and B_o) as iteration progresses as well as for other non-linear terms.

Further, we find the weight forms of Eq. (76) as

$$
\begin{aligned}
0 &= \int_\Omega w_1(\mu(Q+\chi_{1,22}) - A_0\chi_{2,2} + B_0\chi_{2,1} - CQ_{,11} + \lambda(QF_0F_0 + \chi_{1,22}D_0D_0 + 2C_0\chi_{2,21}F_0 \\
&\quad +2E_0\chi_{2,12}D_0 - \chi_{1,21}D_0F_0 - \chi_{1,12}F_0D_0 - E_0RF_0 - C_0\chi_{2,22}D_0 - E_0D_0\chi_{2,21} \\
&\quad -C_0F_0\chi_{2,12}) - \frac{1}{2}Ew_1Q + \frac{1}{2}Ew_1(3QC_0^2 + QD_0^2 + 2RC_0D_0))d\Omega \\
0 &= \int_\Omega w_2(\mu(R+\chi_{2,22}) - B_0\chi_{1,1} + A_0\chi_{1,2} - CR_{,11} + \lambda(RE_0E_0 + \chi_{2,22}C_0C_0 + 2D_0\chi_{1,21}E_0 \\
&\quad +2F_0\chi_{1,12}C_0 - \chi_{2,21}C_0E_0 - \chi_{2,12}E_0C_0 - F_0QE_0 - D_0\chi_{1,22}C_0 - F_0C_0\chi_{1,21} \\
&\quad -D_0E_0\chi_{1,12}) - \frac{1}{2}Ew_2R + \frac{1}{2}w_2E(3RD_0^2 + RC_0^2 + 2QD_0C_0))d\Omega \\
0 &= \int_\Omega w_3(Q-\chi_{1,11})d\Omega, \\
0 &= \int_\Omega w_4(R-\chi_{2,11})d\Omega, \\
0 &= \int_\Omega w_5(C-\chi_{1,1})d\Omega, \\
0 &= \int_\Omega w_6(D-\chi_{2,1})d\Omega, \\
0 &= \int_\Omega w_7(E-\chi_{1,2})d\Omega, \\
0 &= \int_\Omega w_8(F-\chi_{2,2})d\Omega, \\
0 &= \int_\Omega w_9(A_0 - \mu(Q+\chi_{1,22}) - CQ_{,11})d\Omega,
\end{aligned}
$$

$$0 = \int_{\Omega} w_{10}(B_0 - \mu(R + \chi_{2,22}) - CR_{,11})d\Omega, \tag{78}$$

Hence, applying integration by part and Green-stokes theorem, (e.g . $\mu \int_{\Omega^e} w_1 \chi_{1,22} d\Omega = -\mu \int_{\Omega^e} w_{1,2}\chi_{1,2} d\Omega + \mu \int_{\partial\Gamma} w_1 \chi_{1,2} N d\Gamma$) the final weak forms of Eq. (78) can be obtained as follows

$$\begin{aligned}
0 = &\int_{\Omega} (w_1\mu Q - \mu w_{1,2}\chi_{1,2} - w_1 A_0 \chi_{2,2} + w_1 B_0 \chi_{2,1} + C w_{1,1} Q_{,1} + \lambda w_1 Q F_0 F_0 - \lambda w_{1,2}\chi_{1,2} D_0 D_0 \\
&-2\lambda w_{1,1} C_0 \chi_{2,2} F_0 - 2\lambda w_{1,2} E_0 \chi_{2,1} D_0 + \lambda w_{1,1}\chi_{1,2} D_0 F_0 + \lambda w_{1,2}\chi_{1,1} F_0 D_0 - \lambda w_1 E_0 R F_0 \\
&+\lambda w_{1,2} C_0 \chi_{2,2} D_0 + \lambda w_{1,1} E_0 D_0 \chi_{2,2} + \lambda w_{1,2} C_0 F_0 \chi_{2,1} + \frac{1}{2} E w_1 Q \\
&+\frac{1}{2} E w_1 (3QC_0^2 + QD_0^2 + 2RC_0 D_0)) d\Omega + \int_{\partial\Gamma} \mu w_1 \chi_{1,2} N d\Gamma - \int_{\partial\Gamma} C w_1 Q_{,1} N d\Gamma \\
&+ \int_{\partial\Gamma} \lambda w_1 \chi_{1,2} D_0 D_0 N d\Gamma + 2\int_{\partial\Gamma} \lambda w_1 C_0 \chi_{2,2} F_0 N d\Gamma + 2\int_{\partial\Gamma} \lambda w_1 E_0 \chi_{2,1} D_0 N d\Gamma \\
&- \int_{\partial\Gamma} \lambda w_1 \chi_{1,2} D_0 F_0 N d\Gamma - \int_{\partial\Gamma} \lambda w_1 C_0 \chi_{2,2} D_0 N d\Gamma - \int_{\partial\Gamma} \lambda w_1 E_0 D_0 \chi_{2,2} N d\Gamma \\
&- \int_{\partial\Gamma} \lambda w_1 C_0 F_0 \chi_{2,1} N d\Gamma - \int_{\partial\Gamma} \lambda w_1 \chi_{1,1} F_0 D_0 N d\Gamma \\
0 = &\int_{\Omega} (w_2\mu R - \mu w_{2,2}\chi_{2,2} - w_2 B_0 \chi_{1,1} + w_2 A_0 \chi_{1,2} + C w_{2,1} R_{,1} + \lambda w_2 R E_0 E_0 - \lambda w_{2,2}\chi_{2,2} C_0 C_0 \\
&-2\lambda w_{2,1} D_0 \chi_{1,2} E_0 - 2\lambda w_{2,2} F_0 \chi_{1,1} C_0 + \lambda w_{2,1}\chi_{2,2} C_0 E_0 + \lambda w_{2,2}\chi_{2,1} E_0 C_0 - \lambda w_2 F_0 Q E_0 \\
&+\lambda w_{2,2} D_0 \chi_{1,2} C_0 + \lambda w_{2,1} F_0 C_0 \chi_{1,2} + \lambda w_{2,2} D_0 E_0 \chi_{1,1} - \frac{1}{2} E w_2 R \\
&+\frac{1}{2} w_2 E (3RD_0^2 + RC_0^2 + 2QD_0 C_0)) d\Omega + \int_{\partial\Gamma} \mu w_2 \chi_{2,2} N d\Gamma - \int_{\partial\Gamma} C w_2 R_{,1} N d\Gamma \\
&+ \int_{\partial\Gamma} \lambda w_2 \chi_{2,2} C_0 C_0 N d\Gamma + 2\int_{\partial\Gamma} \lambda w_2 D_0 \chi_{1,2} E_0 N d\Gamma + 2\int_{\partial\Gamma} \lambda w_2 F_0 C_0 \chi_{1,1} N d\Gamma \\
&- \int_{\partial\Gamma} \lambda w_2 \chi_{2,2} C_0 E_0 N d\Gamma - \int_{\partial\Gamma} \lambda w_2 F_0 C_0 \chi_{1,2} N d\Gamma - \int_{\partial\Gamma} \lambda w_2 \chi_{2,1} E_0 C_0 N d\Gamma \\
&- \int_{\partial\Gamma} \lambda w_2 D_0 \chi_{1,2} C_0 N d\Gamma - \int_{\partial\Gamma} \lambda w_2 D_0 E_0 \chi_{1,1} N d\Gamma \\
0 = &\int_{\Omega} (w_3 Q + w_{3,1}\chi_{1,1}) d\Omega - \int_{\partial\Gamma} w_3 \chi_{1,1} N d\Gamma \\
0 = &\int_{\Omega} (w_4 R + w_{4,1}\chi_{2,1}) d\Omega - \int_{\partial\Gamma} w_{4,1}\chi_{2,1} N d\Gamma \\
0 = &\int_{\Omega} (w_5 C - w_5 \chi_{1,1}) d\Omega \\
0 = &\int_{\Omega} (w_6 D - w_6 \chi_{2,1}) d\Omega, \\
0 = &\int_{\Omega} (w_7 E - w_7 \chi_{1,2}) d\Omega, \\
0 = &\int_{\Omega} (w_8 F - w_8 \chi_{2,2}) d\Omega, \\
0 = &\int_{\Omega} (w_9 A - \mu w_9 Q + \mu w_{9,2}\chi_{1,2} + C w_{9,1} Q_{,1}) d\Omega - \int_{\partial\Gamma} \mu w_9 \chi_{1,2} N d\Gamma - \int_{\partial\Gamma} C w_9 Q_{,1} N d\Gamma \\
0 = &\int_{\Omega} (w_{10} B - \mu w_{10} R + \mu w_{10,2}\chi_{2,2} + C w_{10,1} R_{,1}) d\Omega - \int_{\partial\Gamma} \mu w_{10}\chi_{2,2} N d\Gamma - \int_{\partial\Gamma} C w_{10} R_{,1} N d\Gamma,
\end{aligned} \tag{79}$$

where Ω, $\partial\Gamma$ and N are, respectively the domain of interest, the associated boundary, and the rightward unit normal to the boundary $\partial\Gamma$ in the sense of the Green-stoke's theorem. The unknowns, χ_1, χ_2, Q, R, C, D, E, F, A and B can be written in the form of Lagrangian

polynomial such that

$$(*) = \sum_{j=1}^{n=4}[(*)_j \Psi_j(x,y)]. \tag{80}$$

Thus, the test function w is found to be

$$w = \sum_{i=1}^{n=4} w_i \Psi_i(x,y);\ \ i = 1,2,3,4,\ \text{and}\ \ j = 1,2,3,4, \tag{81}$$

where w_i is weight of the test function and $\Psi_i(x, y)$ are the shape functions; $\Psi_1 = \frac{(x-2)(y-1)}{2}$, $\Psi_2 = \frac{x(y-1)}{-2}$, $\Psi_3 = \frac{xy}{2}$ and $\Psi_4 = \frac{y(x-2)}{-2}$. By means of Eq. (80), Eq. ((79) may be recast in terms of Lagrangian polynomial as

$$\begin{aligned}
0 = {} & \sum\{\int_{\Omega^e} (\lambda\Psi_{i,1}\Psi_{j,2}D_0F_0 + \lambda\Psi_{i,2}\Psi_{j,1}F_0D_0 - \mu\Psi_{i,2}\Psi_{j,2} - \lambda\Psi_{i,2}\Psi_{j,2}D_0D_0)d\Omega\}\chi_{1j} + \sum\{\int_{\Omega^e} (\Psi_i\Psi_{j,1}B_0 \\
& -\Psi_i\Psi_{j,2}A_0 - 2\lambda\Psi_{i,1}\Psi_{j,2}C_0F_0 - 2\lambda\Psi_{i,2}\Psi_{j,1}E_0D_0 + \lambda\Psi_{i,2}\Psi_{j,2}C_0D_0 + \lambda\Psi_{i,1}\Psi_{j,2}E_0D_0 + \lambda\Psi_{i,2}\Psi_{j,1}C_0F_0)d\Omega\}\chi_{2j} \\
& + \sum\{\int_{\Omega^e} (\mu\Psi_i\Psi_j + C\Psi_{i,1}\Psi_{j,1} + \lambda\Psi_i\Psi_jF_0F_0 + \frac{1}{2}E\Psi_i\Psi_j + \frac{3}{2}E\Psi_i\Psi_jC_0^2 + \frac{1}{2}E\Psi_i\Psi_jD_0^2)d\Omega\}Q_j \\
& + \sum\{\int_{\Omega^e} (-\lambda\Psi_i\Psi_jE_0F_0 + E\Psi_i\Psi_jC_0D_0)d\Omega\}R_j + \int_{\partial\Gamma} (\mu\Psi_i\chi_{1,2})Nd\Gamma - \int_{\partial\Gamma} (C\Psi_iQ_{,1})Nd\Gamma + \int_{\partial\Gamma} (\lambda\Psi_i\chi_{1,2}D_0D_0)Nd\Gamma \\
& + \int_{\partial\Gamma} (2\lambda\Psi_iC_0\chi_{2,2}F_0)Nd\Gamma + 2\int_{\partial\Gamma} (\lambda\Psi_iE_0D_0\chi_{2,1})Nd\Gamma - \int_{\partial\Gamma} (\lambda\Psi_i\chi_{1,2}D_0F_0)Nd\Gamma - \int_{\partial\Gamma} (\lambda\Psi_iC_0\chi_{2,2}D_0)Nd\Gamma \\
& - \int_{\partial\Gamma} (\lambda\Psi_iE_0D_0\chi_{2,2})Nd\Gamma - \int_{\partial\Gamma} (\lambda\Psi_iC_0F_0\chi_{2,1})Nd\Gamma - \int_{\partial\Gamma} (\lambda\Psi_i\chi_{1,1}F_0D_0)Nd\Gamma \\
0 = {} & \sum\{\int_{\Omega^e} (-\Psi_i\Psi_{j,1}B_0 + \Psi_i\Psi_{j,2}A_0 - 2\lambda\Psi_{i,1}\Psi_{j,2}D_0E_0 - 2\lambda\Psi_{i,2}\Psi_{j,1}F_0C_0\lambda\Psi_{i,2}\Psi_{j,2}D_0C_0 + \lambda\Psi_{i,1}\Psi_{j,2}F_0C_0 \\
& + \lambda\Psi_{i,2}\Psi_{j,1}D_0E_0)d\Omega\}\chi_{1j} + \sum\{\int_{\Omega^e} (-\mu\Psi_{i,2}\Psi_{j,2} - \lambda\Psi_{i,2}\Psi_{j,2}C_0C_0 + \lambda\Psi_{i,1}\Psi_{j,2}C_0E_0 + \lambda\Psi_{i,2}\Psi_{j,1}E_0C_0)d\Omega\}\chi_{2j} \\
& + \sum\{\int_{\Omega^e} (-\lambda\Psi_i\Psi_jF_0E_0 + E\Psi_i\Psi_jC_0D_0)d\Omega\}Q_j + \sum\{\int_{\Omega^e} (\mu\Psi_i\Psi_j + C\Psi_{i,1}\Psi_{j,1} + \lambda\Psi_i\Psi_jE_0E_0 + \frac{1}{2}E\Psi_i\Psi_j \\
& + \frac{3}{2}E\Psi_i\Psi_jD_0^2 + \frac{1}{2}E\Psi_i\Psi_jC_0^2)d\Omega\}R_j + \int_{\partial\Gamma} (\mu\Psi_i\chi_{2,2})Nd\Gamma - \int_{\partial\Gamma} (C\Psi_iR_{,1})Nd\Gamma + \int_{\partial\Gamma} (\lambda\Psi_i\chi_{2,2}C_0C_0)Nd\Gamma \\
& + 2\int_{\partial\Gamma} (\lambda\Psi_iD_0\chi_{1,2}E_0)Nd\Gamma + 2\int_{\partial\Gamma} (\lambda\Psi_iF_0C_0\chi_{1,1})Nd\Gamma - \int_{\partial\Gamma} (\lambda\Psi_i\chi_{2,2}C_0E_0)Nd\Gamma - \int_{\partial\Gamma} (\lambda\Psi_i\chi_{2,1}E_0C_0)Nd\Gamma \\
& - \int_{\partial\Gamma} (\lambda\Psi_iD_0\chi_{1,2}C_0)Nd\Gamma - \int_{\partial\Gamma} (\lambda\Psi_iD_0E_0\chi_{1,1})Nd\Gamma - \int_{\partial\Gamma} (\lambda\Psi_iF_0C_0\chi_{1,2})Nd\Gamma \\
0 = {} & \sum\{\int_{\Omega^e} (\Psi_i\Psi_j)d\Omega\}Q_j + \sum\{\int_{\Omega^e} \Psi_{i,1}\Psi_{j,1})d\Omega\}\chi_{1j} - \int_{\partial\Gamma^e} (\Psi_i\chi_{1,1})Nd\Gamma, \\
0 = {} & \sum\{\int_{\Omega^e} (\Psi_i\Psi_j)d\Omega\}R_j + \sum\{\int_{\Omega^e} \Psi_{i,1}\Psi_{j,1})d\Omega\}\chi_{2j} - \int_{\partial\Gamma^e} (\Psi_i\chi_{2,1})Nd\Gamma, \\
0 = {} & \sum\{\int_{\Omega^e} (\Psi_i\Psi_j)d\Omega\}C_j - \sum\{\int_{\Omega^e} (\Psi_i\Psi_{j,1})d\Omega\}\chi_{1j} \\
0 = {} & \sum\{\int_{\Omega^e} (\Psi_i\Psi_j)d\Omega\}D_j - \sum\{\int_{\Omega^e} (\Psi_i\Psi_{j,1})d\Omega\}\chi_{2j} \\
0 = {} & \sum\{\int_{\Omega^e} (\Psi_i\Psi_j)d\Omega\}E_j - \sum\{\int_{\Omega^e} (\Psi_i\Psi_{j,2})d\Omega\}\chi_{1j} \\
0 = {} & \sum\{\int_{\Omega^e} (\Psi_i\Psi_j)d\Omega\}F_j - \sum\{\int_{\Omega^e} (\Psi_i\Psi_{j,2})d\Omega\}\chi_{2j} \\
0 = {} & \sum\{\int_{\Omega^e} (\Psi_i\Psi_j)d\Omega\}A_j + \sum\{\int_{\Omega^e} (-\mu\Psi_i\Psi_j + C\Psi_{i,1}\Psi_{j,1})d\Omega\}Q_j + \sum\{\int_{\Omega^e} (\mu\Psi_{i,2}\Psi_{j,2})d\Omega\}\chi_{1j}
\end{aligned}$$

Table 1
Maximum numerical errors with respect to the number of iterations.

Number of iterations	Maximum error
1	$1.2e-01$
5	$6.4e-02$
10	$3.4e-03$
15	$1.4e-04$
20	$4.1e-05$

$$-\int_{\partial\Gamma^e}(\mu\Psi_i\chi_{1,2})Nd\Gamma-\int_{\partial\Gamma}(C\Psi_iQ_{,1})Nd\Gamma$$

$$0=\sum\{\int_{\Omega^e}(\Psi_i\Psi_j)d\Omega\}B_j+\sum\{\int_{\Omega^e}(-\mu\Psi_i\Psi_j+C\Psi_{i,1}\Psi_{j,1})d\Omega\}R_j+\sum\{\int_{\Omega^e}(\mu\Psi_{i,2}\Psi_{j,2})d\Omega\}\chi_{2j}$$
$$-\int_{\partial\Gamma^e}(\mu\Psi_i\chi_{2,2})Nd\Gamma-\int_{\partial\Gamma}(C\Psi_iR_{,1})Nd\Gamma \tag{82}$$

Now, for the local stiffness matrices and forcing vectors for each elements, we find

$$\begin{bmatrix}K_{11}^{11}&K_{12}^{11}&K_{13}^{11}&K_{14}^{11}\\K_{21}^{11}&K_{22}^{11}&K_{23}^{11}&K_{24}^{11}\\K_{31}^{11}&K_{32}^{11}&K_{33}^{11}&K_{34}^{11}\\K_{41}^{11}&K_{42}^{11}&K_{43}^{11}&K_{44}^{11}\end{bmatrix}_{Local}\begin{bmatrix}\chi_1^1\\\chi_1^2\\\chi_1^3\\\chi_1^4\end{bmatrix}_{Local}=\begin{bmatrix}F_1^1\\F_2^1\\F_3^1\\F_4^1\end{bmatrix}_{Local}, \tag{83}$$

where

$$\left[K_{ij}^{11}\right]=\int_{\Omega}(\lambda\Psi_{i,1}\Psi_{j,2}D_0F_0+\lambda\Psi_{i,2}\Psi_{j,1}F_0D_0-\mu\Psi_{i,2}\Psi_{j,2}-\lambda\Psi_{i,2}\Psi_{j,2}D_0D_0)d\Omega, \tag{84}$$

and

$$\{F_i^1\}=\int_{\partial\Gamma}\mu w_i\chi_{1,2}Nd\Gamma-\int_{\partial\Gamma}Cw_iQ_{,1}Nd\Gamma+\int_{\partial\Gamma}\lambda w_i\chi_{1,2}D_0D_0Nd\Gamma+2\int_{\partial\Gamma}\lambda w_iC_0\chi_{2,2}F_0Nd\Gamma$$
$$+2\int_{\partial\Gamma}\lambda w_iE_0\chi_{2,1}D_0Nd\Gamma-\int_{\partial\Gamma}\lambda w_i\chi_{1,2}D_0F_0Nd\Gamma-\int_{\partial\Gamma}\lambda w_iC_0\chi_{2,2}D_0Nd\Gamma$$
$$-\int_{\partial\Gamma}\lambda w_iE_0D_0\chi_{2,2}Nd\Gamma-\int_{\partial\Gamma}\lambda w_iC_0F_0\chi_{2,1}Nd\Gamma-\int_{\partial\Gamma}\lambda w_i\chi_{1,1}F_0D_0Nd\Gamma. \tag{85}$$

Thus, the unknowns (i.e. χ_1, χ_2, Q, R, C, D, E, F, A and B) can be expressed as

$$Q_i=\{\chi_1^i\}_{,11},\ R_i=\{\chi_2^i\}_{,11},\ S_i=\{Q^i\}_{,11}\ \text{etc...}, \tag{86}$$

and so on for the rest of the unknowns.

Consequently, we obtain the following systems of equations (in the Global form) for each individual elements as

$$\begin{bmatrix}[K^{11}]&[K^{12}]&[K^{13}]&[K^{14}]&[K^{15}]&[K^{16}]&[K^{17}]&[K^{18}]&[K^{19}]&[K^{110}]\\[K^{21}]&[K^{22}]&[K^{23}]&[K^{24}]&[K^{25}]&[K^{26}]&[K^{27}]&[K^{28}]&[K^{29}]&[K^{210}]\\[K^{31}]&[K^{32}]&[K^{33}]&[K^{34}]&[K^{35}]&[K^{36}]&[K^{37}]&[K^{38}]&[K^{39}]&[K^{310}]\\[K^{41}]&[K^{42}]&[K^{43}]&[K^{44}]&[K^{45}]&[K^{46}]&[K^{47}]&[K^{48}]&[K^{49}]&[K^{410}]\\[K^{51}]&[K^{52}]&[K^{53}]&[K^{54}]&[K^{55}]&[K^{56}]&[K^{57}]&[K^{58}]&[K^{59}]&[K^{510}]\\[K^{61}]&[K^{62}]&[K^{63}]&[K^{64}]&[K^{65}]&[K^{66}]&[K^{67}]&[K^{68}]&[K^{69}]&[K^{610}]\\[K^{71}]&[K^{72}]&[K^{73}]&[K^{74}]&[K^{75}]&[K^{76}]&[K^{77}]&[K^{78}]&[K^{79}]&[K^{710}]\\[K^{81}]&[K^{82}]&[K^{83}]&[K^{84}]&[K^{85}]&[K^{86}]&[K^{87}]&[K^{88}]&[K^{89}]&[K^{810}]\\[K^{91}]&[K^{92}]&[K^{93}]&[K^{94}]&[K^{95}]&[K^{96}]&[K^{97}]&[K^{98}]&[K^{99}]&[K^{910}]\\[K^{101}]&[K^{102}]&[K^{103}]&[K^{104}]&[K^{105}]&[K^{106}]&[K^{107}]&[K^{108}]&[K^{109}]&[K^{1010}]\end{bmatrix}\begin{bmatrix}\chi_1^i\\\chi_2^i\\Q_i\\R_i\\A_i\\B_i\\C_i\\D_i\\E_i\\F_i\end{bmatrix}=\begin{bmatrix}\{F_1\}\\\{F_2\}\\\{F_3\}\\\{F_4\}\\\{F_5\}\\\{F_6\}\\\{F_7\}\\\{F_8\}\\\{F_9\}\\\{F_{10}\}\end{bmatrix}. \tag{87}$$

In the simulation, we set the following convergence criteria:

$$|A_{n+1}-A_n|=e_1\le\varepsilon,\ |B_{n+1}-B_n|=e_2\le\varepsilon\ \text{and}\ \varepsilon=\text{maximum error}=10^{-4}, \tag{88}$$

which demonstrates fast convergence within 20 iterations (see, Table. 1).

References

Abe, H., Hayashi, K., 1996. in data book on mechanical properties of living cells. In: Sato, M. (Ed.), Tissues, and Organs. Springer, Tokyo, p. 106.

Antman, S.S., 2005. Nonlinear Problems of Elasticity. Springer, Berlin.

Bailly, L., Toungara, M., Orgéas, L., Bertrand, E., Deplano, V., Geindreau, C., 2014. In-plane mechanics of soft architectured fibre-reinforced silicone rubber membranes. J. Mech. Behav. Biomed.Mater. 1 (40), 339–353.

Bouillaguet, S., Schütt, A., Alander, P., Schwaller, P., Buerki, G., Michler, J., Cattani-Lorente, M., Vallittu, P.K., Krejci, I., 2006. Hydrothermal and mechanical stresses degrade fiber–matrix interfacial bond strength in dental fiber-reinforced composites. J. Biomed. Mater. Res. Part B Appl. Biomater. 76 (1), 98–105.

Cheng, M.Y., Tsao, C.M., Yang, Y.J., 2010. An anthropomorphic robotic skin using highly twistable tactile sensing array. In: 2010 5th IEEE Conference on Industrial Electronics and Applications. IEEE, pp. 650–655.

dell'Isola, F., Corte, A.D., Giorgio, I., 2016. Higher-602 gradient continua: the legacy of Piola, Mindlin, Sedov and Toupin and some 603 future research perspectives. Math. Mech. Solids 22 (4), 852–872.

Dell'Isola, F., Cuomo, M., Greco, L., Della Corte, A., 2017. Bias extension test for pantographic sheets: numerical simulations based on second gradient shear energies. J. Eng. Math. 103 (1), 127–157.

Dell'Isola, F., Della Corte, A., Greco, L., Luongo, A., 2016. Plane bias extension test for a continuum with two inextensible families of fibers: a variational treatment with lagrange multipliers and a perturbation solution. Int. J. Solids Struct. 81, 1–12.

Dell'Isola, F., Giorgio, I., Pawlikowski, M., Rizzi, N.L., 2016. Large deformations of planar extensible beams and pantographic lattices: heuristic homogenization, experimental and numerical examples of equilibrium. In Proc. R. Soc. A 472 (2185).

dell'Isola, F., Seppecher, P., Madeo, A., 2012. How contact interactions may depend on the shape of cauchy cuts in nth gradient 600 continua: approach ?la d'alembert. Z. Angew. Math. Phys. 63, 1119–1141.

Dill, E.H., 1992. Kirchhoff's theory of rods. Arch. Hist. Exact Sci. 44, 1–23.

Fung, Y.C., 1991. What are the residual stresses doing in our blood vessels? Ann Biomed Eng 19, 237–249 https://doi.org/10.1007/BF02584301.

Fung, Y.C., 1993. Biomechanics. Springer, New York, NY, pp. 321–391.

Gent, A.N., 1996. A new constitutive relation for rubber. Rubber Chem. Technol. 69, 59–61.

Germain, P., 2015. The method of virtual power in continuum mechanics, part 2: microstructure. SIAM J. Appl. Math 25, 556–575. (1973) stretching. Acta Mech. Sin. 31(3), 373–382

Holzapfel, G.A., 2008. Collagen in arterial walls: biomechanical aspects. In: Collagen. Springer, Boston, MA, pp. 285–324.

Holzapfel, G.A., Gasser, T.C., Ogden, R.W., 2000. A new constitutive framework for arterial wall mechanics and a comparative study of material models. J. Elasticity 61, 1–48.

Holzapfel, G.A., Ogden, R.W., 2006. Mechanics of Biological Tissue. Springer, Heidelberg.

Javili, A., dell'Isola, F., Steinmann, P., 2013. Geometrically nonlinear higher-gradient elasticity with energetic boundaries. J.Mech. Phys. Solids 61 (12), 2381–2401.

Kim, C., Zeidi, M., 2018. Gradient elasticity theory for fiber composites with fibers resistant to extension and flexure. Int. J. Eng. Sci. 131, 80–99.

Kim, C.I., 2019. Strain-gradient elasticity theory for the mechanics of fiber composites subjected to finite plane deformations. Compr. Anal. Multiscale Sci.Eng. 1 (2), 150–160.

Koiter, W.T., 1964. Couple-stresses in the theory of elasticity. Proc. K. Ned. Akad. Wetensc. B 67, 17–44.

Landau, L.D., Lifshitz, E.M., 1986. Theory of Elasticity. 3rd ed. Pergamon, Oxford.

Leong, K.H., Ramakrishna, S., Huang, Z.M., Bibo, G.A., 2000. The potential of knitting for engineering composites—a review. Compos. Part A 1;31 (3), 197–220.

Lu, T., Huang, J., Jordi, C., Kovacs, G., Huang, R., Clarke, D.R., Suo, Z., 2012. Dielectric elastomer actuators under equal-biaxial forces, uniaxial forces, and uniaxial constraint of stiff fibers. Soft Matter 8, 6167–6173.

Ma, Y., Feng, X., Rogers, J.A., Huang, Y., Zhang, Y., 2017. Design and application of 'Jshaped'stress–strain behavior in stretchable electronics: a review. Lab Chip 17, 1689–1704.

Martinez, R.V., Branch, J.L., Fish, C.R., Jin, L., Shepherd, R.F., Nunes, R.M., Suo, Z., Whitesides, G.M., 2013. Robotic tentacles with three-dimensional mobility based on flexible elastomers. Adv. Mater. 25 (2), 205–212.

Maurer, M., Röhrnbauer, B., Feola, A., Deprest, J., Mazza, E., 2015. Prosthetic meshes for repair of hernia and pelvic organ prolapse: Comparison of biomechanical properties. Materials 8 (5), 2794–2808.

Mihai, L.A., Goriely, A., 2017. How to characterize a nonlinear elastic material? a review on nonlinear constitutive parameters in isotropic finite elasticity. In: Proceedings Royal Society London A.

Mindlin, R.D., Tiersten, H.F., 1962. Effects of couple-stress in linear elasticity. Arch. Rational Mech. Anal. 11, 415.

Mindlin, R.D., Tiersten, H.F., 1962. Effects of couple-stresses in linear elasticity. Arch. Ration. Mech. Anal. 11, 415–448.

Myung, D., Koh, W., Ko, J., Hu, Y., Carrasco, M., Noolandi, J., Ta, C.N., Frank, C.W., 2007. Biomimetic strain hardening in interpenetrating polymer network hydrogels. Polymer 48, 5376–5387.

Ogden, R.W., 1984. Non-Linear Elastic Deformations. Ellis Horwood Ltd., Chichester, England.

Pritts, M.B., Rahn, C.D., 2004. Design of an artificial muscle continuum robot. In: InIEEE International Conference on Robotics and Automation, 2004. Proceedings. ICRA'04. 2004, Vol. 5. IEEE, pp. 4742–4746.

Rivlin, R.S., 1995. Constitutive equations for a fiber-reinforced lamina. In: Parker, D.F., England, A.H. (Eds.), In IUTAM Symposium on Anisotropy, Inhomogeneity and Nonlinearity in Solid Mechanics. Kluwer Academic Publishers, Dordrecht, pp. 379–384.

Shadwick, R.E., 1999. J. Exp. Biol. 202, 3305.

Shao, H., Li, J., Chen, N., Shao, G., Jiang, J., Yang, Y., 2018. Experimental study on bi-axial mechanical properties of warp-knitted meshes with and without initial notches. Materials. 11 (10). 1999

Spencer, A.J.M., 1972. Deformations of Fibre-reinforced Materials. Oxford University, Press, London.

Spencer, A.J.M., 1984. Continuum theory of the mechanics of fibre reinforced composites. CISM Courses and Lectures No.282. Springer Verlag, Wien.

Spencer, A.J.M., Soldatos, K.P., 2007. Finite deformations of fibre-reinforced elastic solids with fibre bending stiffness. Int. J. Non-Linear Mech 42, 355–368.

Steigmann, D.J., 2002. Invariants of the stretch tensors and their application to finite elasticity theory. Math. Mech. Solids 7, 393–404.

Steigmann, D.J., 2012. Theory of elastic solids reinforced with fibers resistant to extension, flexure and twist. Int. J. Non-Linear Mech. 47, 734–742.

Steigmann, D.J., 2017. Finite Elasticity Theory. Oxford University Press, Oxford, United Kingdom.

Steigmann, D.J., dell'Isola, F., 2015. Mechanical response of fabric sheets to three-dimensional bending, twisting, and stretching. Acta Mech. Sin. 31 (3), 373–382.

Toupin, R.A., 1962. Elastic materials with couple-stress. Arch. Rational Mech. Anal 11, 385.

Toupin, R.A., 1964. Theories of elasticity with couple stress. Arch. Ration. Mech. Anal 17, 85–112.

Truesdell, C., Noll, W., 1965. The non-linear field theories of mechanics. In: Flugge, S. (Ed.), Handbuch der Physik, vol. III/3. Springer, Berlin.

Vatankhah-Varnosfaderani, M., Daniel, W.F., Everhart, M.H., Pandya, A.A., Liang, H., Matyjaszewski, K., Dobrynin, A.V., Sheiko, S.S., 2017. Nature 549, 497.

Wang, Y., Gregory, C., Minor, M.A., 2018. Improving mechanical properties of molded silicone rubber for soft robotics through fabric compositing. Soft Robot. 5 (3), 272–290.

Yan, B., Huang, J., Han, L., Gong, L., Li, L., Israelachvili, J.N., Zeng, H., 2017. Duplicating dynamic strain-stiffening behavior and nanomechanics of biological tissues in a synthetic self-healing flexible network hydrogel. ACS nano 11, 11074–11081.

Zeidi, M., Kim, C., 2017. Finite plane deformations of elastic solids reinforced with fibers resistant to flexure: complete solution. Arch. Appl. Mech. doi:10.1007/s00419-018-1344-3.

Zeidi, M., Kim, C., 2017. Mechanics of fiber composites with fibers resistant to extension and flexure. Math. Mech. Solids doi:10.7939/R3Z892V17.

Zeidi, M., Kim, C., 2018. Mechanics of an elastic solid reinforced with bidirectional fiber in finite plane elastostatics: complete analysis. Continuum Mech. Thermodyn doi:10.1007/s00161-018-0623-0.

Zhalmuratova, D., La, T.-G., Yu, K., Szojka, A., Andrews, S., Adesida, A. B., Kim, C.-i., Nobes, D., Freed, D., Chung, H.-J.,. "mimicking 'j-shaped' and anisotropic stress-strain behavior of human and porcine aorta by fabric-reinforced elastomer composites". In: ACS Applied Materials & Interfaces. 10.1021/acsami.9b10524

Zhao, X., Wang, Q., 2014. Harnessing large deformation and instabilities of soft dielectrics: theory, experiment, and application. Appl. Phys. Rev. 1, 21304.